

Full-Covariance Chemical Langevin Predator–Prey Diffusion with Absorbing Boundaries

Jiguang Yu^{1†}, Louis Shuo Wang^{2*†}, Yuansheng Gao³, Ye Liang⁴

¹College of Engineering, Boston University, Boston, 02215, MA, USA.

²Department of Mathematics, University of Tennessee, Knoxville, 37996, TN, USA.

³College of Computer Science and Technology, Zhejiang University, Hangzhou, 310000, Zhejiang, China.

⁴Department of Industrial and Systems Engineering, The University of Iowa, Iowa City, 52242, IA, USA.

*Corresponding author(s). E-mail(s): swang116@vols.utk.edu;
Contributing authors: jyu678@bu.edu; y.gao@zju.edu.cn;
ye-liang@uiowa.edu;

†These authors contributed equally to this work as co-first authors.

Abstract

Many stochastic predator–prey models for Rosenzweig–MacArthur dynamics add ad hoc independent (diagonal) noise, which cannot encode the event-level coupling created by predation and biomass conversion. We develop a fully mechanistic route from elementary reactions to an absorbed diffusion approximation and its extinction structure. Starting from a continuous-time Markov chain on \mathbb{N}_0^2 with four reaction channels, including prey birth, prey competition death, predator death, and a coupled predation–conversion event, we impose absorbing coordinate axes, capturing the irreversibility of demographic extinction. Under Kurtz density-dependent scaling, the law-of-large-numbers limit recovers the classical Rosenzweig–MacArthur ordinary differential equation, while central-limit scaling yields a chemical-Langevin diffusion with explicit drift and a full state-dependent covariance matrix. A key structural feature is the strictly negative instantaneous cross-covariance $\Sigma_{12}(N, P) = -mNP/(1 + N)$, arising uniquely from the predation–conversion increment $(-1, 1)$ and absent from diagonal-noise surrogates. We provide two equivalent Brownian representations: an event-based factorization with a four-dimensional driver preserving reaction channels, and a two-dimensional Cholesky factorization convenient for simulation. Defining the absorbed Itô SDE by freezing trajectories at the first boundary

hit, we prove strong existence, pathwise uniqueness, non-explosion, and uniform moment bounds up to absorption. Extinction occurs with positive probability from every interior state, and predator extinction is almost sure in the subcritical regime $m \leq c$. Reproducible Euler–Maruyama diagnostics validate factorization consistency and quantify the effect of the cross-covariance in representative parameter regimes.

Keywords: density-dependent Markov chain; chemical Langevin equation; absorbed diffusion (absorbing boundary); predator–prey model (Rosenzweig–MacArthur); demographic stochasticity; extinction (hitting time)

1 Introduction

Extinction is an intrinsically irreversible event in finite populations: once one species' count hits zero, there is no endogenous mechanism that recreates it. At the individual (demographic) level, this irreversibility is naturally encoded by a continuous-time Markov chain (CTMC) on \mathbb{N}_0^2 . In this model, the coordinate axes are absorbing sets. There are no births in the absence of individuals, and no predation or conversion events unless both species are present.

Such absorption and extinction mechanisms are standard in stochastic population models; see, for example, the general discussions in (Allen 2015; Ovaskainen and Meerson 2010; Nåsell 2001; Lande et al. 2003). Such Markov chain models are frequently investigated through sample-path simulations to obtain Monte Carlo estimates of quantities of interest (Gibson and Bruck 2000; Gillespie 1976; Korner-Nievergelt et al. 2015; Hobolth and Stone 2009). In the diffusion approximation developed here, we adopt the same biological convention by imposing absorption at the coordinate axes. Once the diffusion reaches $\{N = 0\} \cup \{P = 0\}$, it is frozen at that state. Consequently, the boundary represents demographic extinction events, rather than reflecting or re-entering behavior.

Deterministically, the Rosenzweig–MacArthur predator–prey system with a Holling type II functional response provides a canonical mean-field backbone for coexistence and predator persistence thresholds (Rosenzweig and MacArthur 1963; Holling 1959; Murray 2002). In the coexistence regime, the model is also a standard setting for enrichment-driven destabilization and oscillatory dynamics (Rosenzweig 1971; Sugie and Saito 2012). However, when demographic stochasticity is incorporated, the form of the noise becomes model-defining: a mechanistic description must reflect that a single predation–conversion event simultaneously decreases prey and increases predators. Consequently, any diffusion approximation derived from such events carries an instantaneous negative cross-covariance in its demographic noise, which is not captured by ad hoc diagonal/independent-noise surrogates. This observation follows directly from the standard reaction-channel (stoichiometric) construction of density-dependent Markov chains and their diffusion (Langevin) approximations (Kurtz 1970, 1971, 1976; Ethier and Kurtz 1986; Gillespie 1977, 2000; Anderson and Kurtz 2011; Kampen 2007). In this framework, the covariance matrix is obtained by summing $\lambda_e(z) \Delta_e \Delta_e^\top$ over

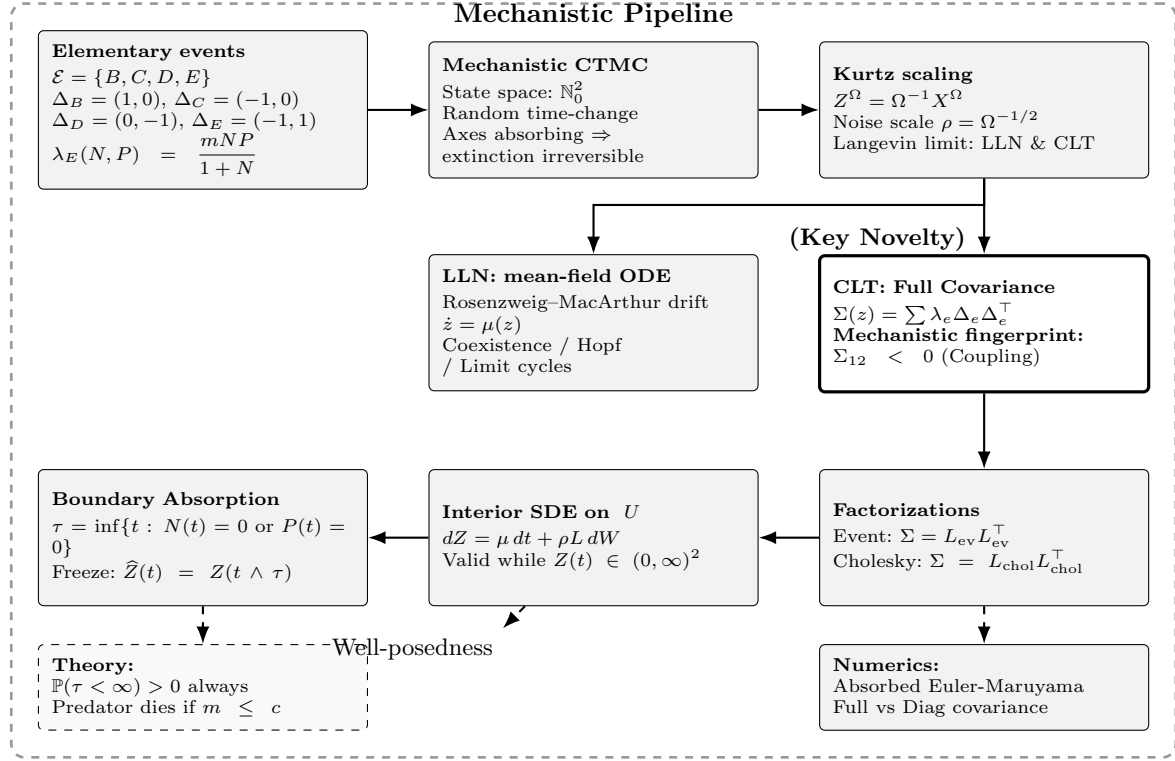


Fig. 1 Mechanistic roadmap. The pipeline proceeds from event-level definition to macroscopic scaling, yielding a full-covariance diffusion with structural signature $\Sigma_{12} < 0$.

all reaction events e . Events that act simultaneously on multiple components therefore generate off-diagonal covariance terms. We illustrate the mechanistic roadmap in Figure 1.

A large fraction of the stochastic predator-prey literature introduces randomness by directly perturbing a deterministic ordinary differential equation (ODE). This is most often done by adding Gaussian (or Lévy) forcing. In practice, the noise typically enters through diagonal multiplicative terms driven by independent Brownian motions, or it acts on a single component only. For example, stochastic Holling-type II predator-prey models are often written in the form

$$dN = \dots dt + \sigma_1 N dB_1, \quad dP = \dots dt + \sigma_2 P dB_2$$

where B_1 and B_2 are independent Brownian motions. This choice yields a diffusion matrix that is diagonal at the level of instantaneous covariation (Zhang 2017; Jiang et al. 2020; Zou et al. 2020; Huang et al. 2021). More generally, reviews and applied studies of noisy consumer-resource cycles often adopt stochastically forced ODEs in which the noise enters through one or several independent exogenous drivers (Barraquand et al. 2017). While such formulations are useful for representing environmental

variability, they do not encode the demographic event structure underlying consumer–resource interactions. As a result, they cannot, by construction, distinguish between noise sources that act independently on each species and those generated by coupled events. In particular, they fail to capture predation-with-conversion events that simultaneously decrease prey abundance and increase predator abundance. Other coupled mechanistic models display Turing patterning, indicating that the absence of coupling structures will result in the loss of critical system behaviors (Liu et al. 2025). In studies that emphasize internal stochasticity in predator–prey SDEs, the stochastic model is typically postulated directly at the SDE level. Analysis is then carried out using Lyapunov techniques (Abundo 1991). By contrast, these models are not derived from an explicit event-based CTMC scaling.

The present paper closes this modeling gap by starting from a mechanistic CTMC specified in terms of elementary demographic events (Figure 2). These events include birth, competition, death, and a predation–conversion channel. We then apply Kurtz’s density-dependent scaling to derive a diffusion approximation with explicit drift and covariance structures. In particular, the coupled predation–conversion event necessarily generates a strictly negative instantaneous cross-covariance, $\Sigma_{12} < 0$, throughout the interior of the state space. This feature is structural: it is absent from diagonal or independent-noise surrogate models. Moreover, it follows directly from the reaction-channel covariance construction $\Sigma(z) = \sum_e \lambda_e(z) \Delta_e \Delta_e^\top$ (Anderson et al. 2019; Leite and Williams 2019). Recent work has developed general SDE-based frameworks for predator–prey models with pure demographic noise. It proves well-posedness and moment/asymptotic bounds and argues that demographic noise alone need not imply extinction (Wang and Yu 2025).

The paper makes the following contributions.

- (C1) (Mechanistic CTMC and density-dependent scaling.) We formulate a prey–predator CTMC on \mathbb{N}_0^2 from four elementary demographic event channels (birth, competition, predation–conversion, and predator death) via a random time-change representation. Under a standard density-dependent scaling in the sense of Kurtz, we obtain the Rosenzweig–MacArthur ODE as the law-of-large-number (LLN) limit and a diffusion approximation under the central-limit-theorem (CLT) scaling with noise amplitude $\rho = \Omega^{-1/2}$.
- (C2) (Full covariance and mechanistic negative correlation.) We compute the limiting drift and the explicit diffusion matrix $\Sigma(N, P)$ implied by the event model. In particular, the coupled predation–conversion channel yields a strictly negative cross-covariance $\Sigma_{12}(N, P) = -\frac{mNP}{1+N} < 0$ on the interior, providing a direct mechanistic signature that is absent from diagonal/independent-noise surrogates. We record two convenient Brownian factorizations: an event-based factorization $\Sigma = L_{\text{ev}} L_{\text{ev}}^\top$ driven by a 4-dimensional Brownian motion, and a 2×2 Cholesky factorization on $(0, \infty)^2$.
- (C3) (Absorbed SDE and well-posedness up to extinction.) We define a full-covariance Itô diffusion on $U = (0, \infty)^2$ and impose absorption at the axes by freezing the trajectory upon first hitting $\partial U = \{N = 0\} \cup \{P = 0\}$. For the resulting absorbed model we prove strong existence and pathwise uniqueness up to the absorption

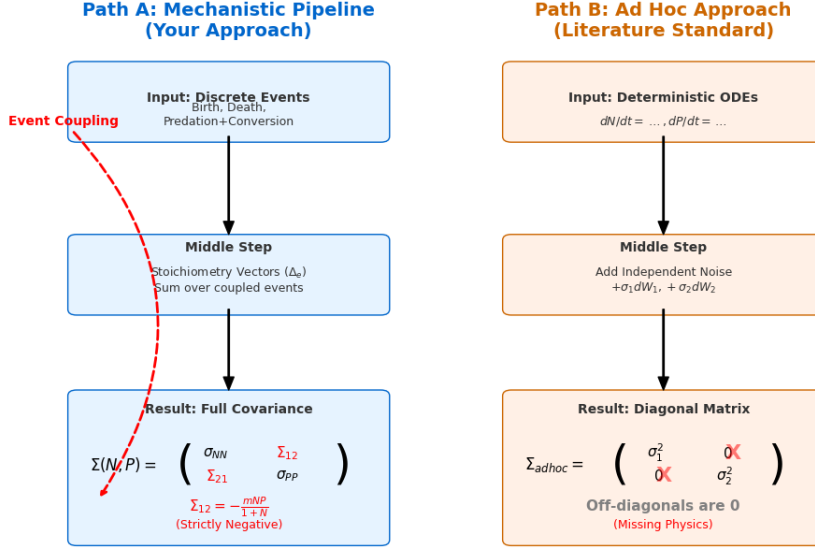


Fig. 2 Mechanistic vs. Ad Hoc Noise. Path A derives the diffusion matrix from demographic events, revealing the intrinsic negative correlation caused by predation. Path B assumes independent noise, missing this structural coupling.

time, together with non-explosion and uniform moment bounds on finite time horizons.

- (C4) (Extinction structure.) We show that extinction occurs with strictly positive probability from every interior initial condition, for all parameter values. Moreover, in the subcritical regime $m \leq c$, predator extinction occurs almost surely, so the absorbed process hits the predator axis in finite time with probability one.
- (C5) (Reproducible numerical diagnostics.) We document Euler–Maruyama (EM) simulation procedures for the absorbed diffusion and provide diagnostics that map directly to the theory: (i) a finite-sample consistency check comparing event-based and Cholesky-based factorizations (4D vs 2D noise), and (ii) a covariance-role comparison between the full mechanistic model and a diagonal surrogate with matched marginal variances.

We collect the main results in a form suitable for quick reference. Throughout, parameters satisfy $k > 0$, $m > 0$, $c > 0$, and the demographic noise amplitude is denoted by $\rho > 0$. Write $U := (0, \infty)^2$ and $\bar{U} := [0, \infty)^2$.

Theorem 1.1 (Mechanistic diffusion and covariance structure) *Consider the mechanistic event model with four channels (prey birth, prey competition death, predator death, and coupled predation–conversion) and the density-dependent scaling $Z^\Omega = \Omega^{-1} X^\Omega$ with $\rho = \Omega^{-1/2}$.*

Then the limiting drift is the Rosenzweig–MacArthur vector field

$$\mu(N, P) = \begin{pmatrix} N - \frac{N^2}{k} - \frac{mNP}{1+N} \\ \frac{mNP}{1+N} - cP \end{pmatrix}, \quad (N, P) \in \mathbb{R}_+^2, \quad (1)$$

and the associated diffusion (instantaneous covariance) matrix is

$$\Sigma(N, P) = \begin{pmatrix} N + \frac{N^2}{k} + \frac{mNP}{1+N} & -\frac{mNP}{1+N} \\ -\frac{mNP}{1+N} & cP + \frac{mNP}{1+N} \end{pmatrix}. \quad (2)$$

In particular, on U one has the strict mechanistic negative correlation $\Sigma_{12}(N, P) = -\frac{mNP}{1+N} < 0$. Moreover, Σ admits an event-based Brownian factorization $\Sigma = L_{\text{ev}} L_{\text{ev}}^\top$ with $L_{\text{ev}} : \overline{U} \rightarrow \mathbb{R}^{2 \times 4}$ given explicitly by the reaction channels, and a 2×2 Cholesky factorization on U .

Theorem 1.2 (Strong well-posedness up to absorption and non-explosion) *Let $z_0 \in U$ and let W be a standard \mathbb{R}^4 Brownian motion. Consider the interior SDE on U driven by the event factor L_{ev} from Theorem 1.1:*

$$dZ(t) = \mu(Z(t)) dt + \rho L_{\text{ev}}(Z(t)) dW(t), \quad Z(0) = z_0, \quad (3)$$

and define the absorption time $\tau := \inf\{t > 0 : Z(t) \notin U\} = \inf\{t > 0 : N(t) = 0 \text{ or } P(t) = 0\}$. Then:

- (i) *There exists a unique (up to indistinguishability) strong solution Z to (3) on $[0, \tau)$.*
- (ii) *The absorbed (frozen) extension $\widehat{Z}(t) := Z(t)$ for $t < \tau$ and $\widehat{Z}(t) := Z(\tau)$ for $t \geq \tau$ is a continuous adapted \overline{U} -valued process and ∂U is absorbing for \widehat{Z} .*
- (iii) *The interior dynamics do not explode prior to absorption: the maximal lifetime equals τ a.s. Moreover, for each $T > 0$ and $p = 2$ or $p \geq 4$ there exists $C_{p,T} < \infty$ such that*

$$\sup_{0 \leq t \leq T} \mathbb{E}[|Z(t \wedge \tau)|^p] \leq C_{p,T} (1 + |z_0|^p).$$

Theorem 1.3 (Extinction properties) *Let \widehat{Z} be the absorbed diffusion from Theorem 1.2.*

- (i) *(Positive extinction probability for all parameters) For every $z \in U$,*

$$\mathbb{P}_z(\tau < \infty) > 0.$$

- (ii) *(Almost sure predator extinction in the subcritical regime) If $m \leq c$, then for every $z \in U$,*

$$\mathbb{P}_z(\inf\{t \geq 0 : P(t) = 0\} < \infty) = 1,$$

and consequently $\mathbb{P}_z(\tau < \infty) = 1$.

Remark 1.4 (Roadmap to proofs). The explicit drift/covariance structure and Brownian factorizations are established in Section 5. Strong well-posedness up to absorption and non-explosion/moment bounds is proved in Section 6. The extinction assertions in Theorem 1.3 are proved in Section 7, with details for the extinction in the subcritical regime deferred to Appendix C and the positive-probability argument deferred to Appendix B.

Section 2 reviews the deterministic Rosenzweig–MacArthur mean-field backbone needed for parameter interpretation and local stability properties. Section 3 specifies the mechanistic CTMC through elementary demographic events. Sections 4–5 introduce the density-dependent scaling, derive the diffusion approximation by identifying the limiting drift and covariance, and record both the event-based (4D) and Cholesky (2D) Brownian factorizations. Section 6 introduces the absorbed (frozen) full-covariance SDE and proves strong well-posedness up to the absorption time, together with non-explosion and moment bounds. Section 7 studies the boundary structure and establishes extinction results, including a positive probability of extinction for all parameters and almost sure predator extinction in the subcritical regime. Section 8 documents numerical schemes and diagnostics supporting the theoretical statements, with emphasis on factorization consistency and the role of the full covariance. We conclude this work in the Discussion Section.

2 Deterministic mean-field backbone

This section records the deterministic Rosenzweig–MacArthur ODE that arises as the LLN limit of the mechanistic CTMC under Kurtz scaling (Section 4). Our purpose here is purely auxiliary. We fix the notation and biologically meaningful state space and record basic invariance and boundedness properties (dissipativity). We also summarize deterministic coexistence versus extinction thresholds for parameter interpretation. We do not pursue the Hopf bifurcation or global planar dynamics in this paper.

We assume

$$k > 0, \quad m > 0, \quad c > 0, \quad (4)$$

and interpret $N(t) \geq 0$ as prey density and $P(t) \geq 0$ as predator density. The biologically meaningful state space is the closed quadrant

$$\bar{U} := \{(N, P) \in \mathbb{R}^2 : N \geq 0, P \geq 0\}, \quad U := \{(N, P) \in \mathbb{R}^2 : N > 0, P > 0\}.$$

For an initial condition $(N_0, P_0) \in \bar{U}$ we consider

$$\begin{cases} \dot{N} = N \left(1 - \frac{N}{k}\right) - \frac{mNP}{1+N}, \\ \dot{P} = P \left(\frac{mN}{1+N} - c\right), \end{cases} \quad (N(0), P(0)) = (N_0, P_0). \quad (5)$$

Let $F : \bar{U} \rightarrow \mathbb{R}^2$ denote the vector field in (5). Note that F is C^∞ on U and locally Lipschitz on \bar{U} .

Lemma 2.1 (Local well-posedness) *For every $(N_0, P_0) \in \bar{U}$, there exists a maximal time $T_{\max} \in (0, \infty]$ and a unique maximal solution*

$$(N, P) \in C^1([0, T_{\max}); \bar{U})$$

to (5). Moreover, the solution depends continuously on the initial data on compact time intervals.

Proof Since F is locally Lipschitz on \overline{U} , existence and uniqueness of a maximal solution follow from the Picard–Lindelöf theorem; continuous dependence is standard. \square

Lemma 2.2 (Positive invariance of \overline{U}) *The closed quadrant \overline{U} is forward invariant for (5). In addition, the coordinate axes are invariant.*

Proof On \overline{U} the predator equation reads $\dot{P} = P\psi(N)$ with $\psi(N) := \frac{mN}{1+N} - c$, hence

$$P(t) = P_0 \exp\left(\int_0^t \psi(N(s)) ds\right) \geq 0, \quad t \in [0, T_{\max}).$$

In particular, if $P_0 = 0$ then $P(t) \equiv 0$. Similarly, writing $\dot{N} = N\phi(N, P)$ with

$$\phi(N, P) := \left(1 - \frac{N}{k}\right) - \frac{mP}{1+N},$$

we obtain

$$N(t) = N_0 \exp\left(\int_0^t \phi(N(s), P(s)) ds\right) \geq 0, \quad t \in [0, T_{\max}).$$

If $N_0 = 0$ then $N(t) \equiv 0$, which forces $P(t) \rightarrow 0$ since $\dot{P} = -cP$ on $\{N = 0\}$. \square

We establish dissipativity of (5) by combining a logistic comparison for N with a linear Lyapunov combination controlling $N + \beta P$. This yields a compact absorbing set in \overline{U} that is independent of the initial condition, and in particular implies global existence.

Lemma 2.3 (Logistic comparison for the prey) *Let (N, P) be the maximal solution to (5) with $(N_0, P_0) \in \overline{U}$. Then*

$$0 \leq N(t) \leq \max\{N_0, k\} \quad \text{for all } t \in [0, T_{\max}). \quad (6)$$

Moreover, for every $\delta > 0$ there exists $T_\delta = T_\delta(N_0) \geq 0$ such that

$$0 \leq N(t) \leq k + \delta \quad \text{for all } t \geq T_\delta \text{ with } t < T_{\max}. \quad (7)$$

Proof Since $P(t) \geq 0$,

$$\dot{N}(t) = N(t)\left(1 - \frac{N(t)}{k}\right) - \frac{mN(t)P(t)}{1+N(t)} \leq N(t)\left(1 - \frac{N(t)}{k}\right).$$

Comparison with $\dot{y} = y(1 - y/k)$ yields (6). The eventual bound (7) follows from the explicit logistic solution: for any $\delta > 0$ the logistic trajectory enters and stays in $[0, k + \delta]$ after some finite time depending only on N_0 . \square

For $\beta \in (0, 1]$, define the linear functional

$$S_\beta(N, P) := N + \beta P. \quad (8)$$

Lemma 2.4 (Absorbing half-space via S_β) Fix $\beta \in (0, 1]$ and let (N, P) solve (5). Then, for all $t \in [0, T_{\max}]$,

$$\frac{d}{dt} S_\beta(N(t), P(t)) \leq \frac{k}{4}(1+c)^2 - c S_\beta(N(t), P(t)). \quad (9)$$

Consequently,

$$S_\beta(N(t), P(t)) \leq S_\beta(N_0, P_0) e^{-ct} + \frac{k(1+c)^2}{4c}(1 - e^{-ct}), \quad t \in [0, T_{\max}), \quad (10)$$

and for every $\varepsilon > 0$ there exists $T_\varepsilon = T_\varepsilon(N_0, P_0) \geq 0$ such that

$$S_\beta(N(t), P(t)) \leq \frac{k(1+c)^2}{4c} + \varepsilon \quad \text{for all } t \geq T_\varepsilon \text{ with } t < T_{\max}. \quad (11)$$

Proof Differentiate S_β along (5):

$$\frac{d}{dt} S_\beta = \dot{N} + \beta \dot{P} = N\left(1 - \frac{N}{k}\right) - \frac{mNP}{1+N} + \beta P\left(\frac{mN}{1+N} - c\right).$$

Rearranging,

$$\begin{aligned} \frac{d}{dt} S_\beta &= N\left(1 - \frac{N}{k}\right) - \beta c P - (1 - \beta) \frac{mNP}{1+N} \leq N\left(1 - \frac{N}{k}\right) - \beta c P \\ &\leq N\left(1 - \frac{N}{k}\right) + cN - cS_\beta = (1+c)N - \frac{N^2}{k} - cS_\beta. \end{aligned}$$

Maximizing the concave quadratic in $N \geq 0$ yields

$$(1+c)N - \frac{N^2}{k} \leq \frac{k}{4}(1+c)^2,$$

which gives (9). Solving the scalar differential inequality yields (10), and (11) follows. \square

For $\delta, \varepsilon > 0$ and $\beta \in (0, 1]$, define the compact set

$$\mathcal{A}_{\beta, \varepsilon, \delta} := \left\{ (N, P) \in \overline{U} : 0 \leq N \leq k + \delta, 0 \leq N + \beta P \leq \frac{k(1+c)^2}{4c} + \varepsilon \right\}. \quad (12)$$

Theorem 2.5 (Dissipativity, absorbing set, and global existence) Fix $\beta \in (0, 1]$ and $\varepsilon, \delta > 0$. For every initial condition $(N_0, P_0) \in \overline{U}$, the corresponding solution of (5) is global, i.e. $T_{\max} = \infty$, and there exists a finite time $T = T(N_0, P_0; \beta, \varepsilon, \delta) \geq 0$ such that

$$(N(t), P(t)) \in \mathcal{A}_{\beta, \varepsilon, \delta} \quad \text{for all } t \geq T.$$

In particular, (5) is dissipative on \overline{U} and admits a uniform absorbing set (independent of the initial condition).

Proof Lemma 2.3 yields that for the given $\delta > 0$ there exists T_1 such that $N(t) \leq k + \delta$ for all $t \geq T_1$. Lemma 2.4 yields that for the given $\varepsilon > 0$ there exists T_2 such that $N(t) + \beta P(t) \leq \frac{k(1+c)^2}{4c} + \varepsilon$ for all $t \geq T_2$. Thus, with $T := \max\{T_1, T_2\}$ we have $(N(t), P(t)) \in \mathcal{A}_{\beta, \varepsilon, \delta}$ for all $t \geq T$.

Finally, since F is locally Lipschitz and solutions remain in the compact set $\mathcal{A}_{\beta, \varepsilon, \delta}$ for all sufficiently large times, no finite-time blow-up can occur. Hence $T_{\max} = \infty$. \square

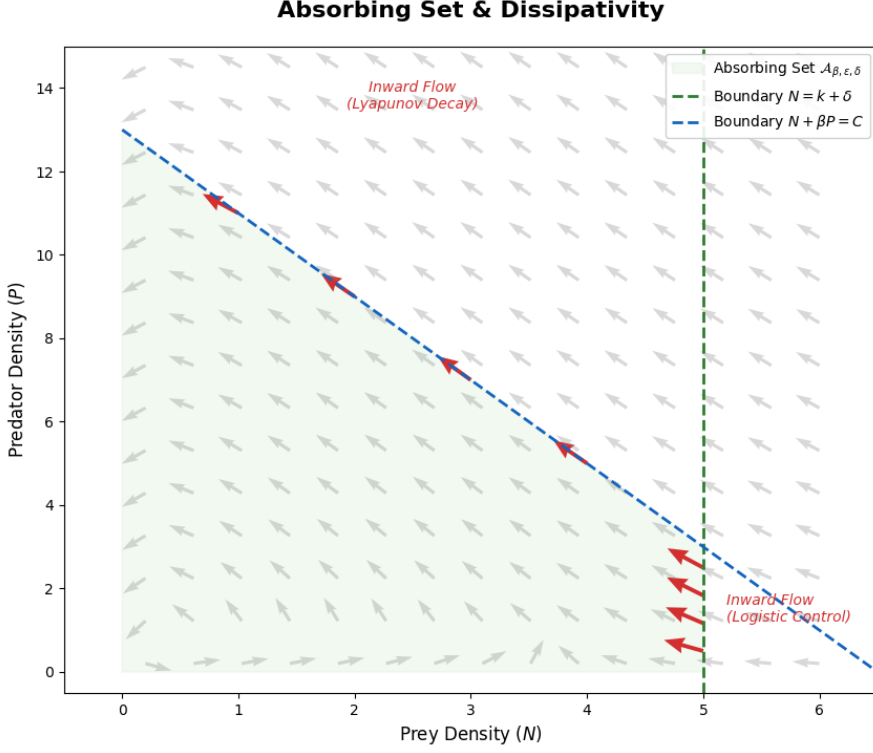


Fig. 3 Visual proof of dissipativity and the absorbing set. Illustration of the compact invariant region $\mathcal{A}_{\beta, \varepsilon, \delta}$ defined in Theorem 2.5. The region (light green) is bounded by the prey logistic constraint $N = k + \delta$ (green dashed line) and the linear Lyapunov constraint $N + \beta P = C$ (blue dashed line). The red arrows along the boundaries explicitly show the inward direction of the vector field. They demonstrate that any trajectory starting outside will eventually enter and remain within this set, thereby ensuring global existence and non-explosion for the deterministic backbone.

Figure 3 shows the absorbing set, providing a visual proof for dissipativity.

We summarize equilibria and deterministic extinction/coexistence thresholds for later parameter interpretation. Define, when $m > c$,

$$N^* := \frac{c}{m - c}. \quad (13)$$

Proposition 2.6 (Equilibria) *The equilibria of (5) in \overline{U} are:*

1. *The origin $K_0 = (0, 0)$.*
2. *The prey-only equilibrium $K_1 = (k, 0)$.*
3. *If $m > c$ and $N^* < k$, there exists a unique coexistence equilibrium*

$$K_3 = (N^*, P^*), \quad P^* := \frac{1 + N^*}{m} \left(1 - \frac{N^*}{k} \right) > 0.$$

If $m \leq c$ or $m > c$ with $N^ \geq k$, then no positive equilibrium exists.*

Proof Equilibria satisfy $\dot{N} = \dot{P} = 0$. From $\dot{P} = P(\frac{mN}{1+N} - c)$ we obtain $P = 0$ or $\frac{mN}{1+N} = c$, the latter equivalent to $N = N^*$ when $m > c$. If $P = 0$, then $\dot{N} = N(1 - N/k)$ gives $N \in \{0, k\}$. If $m > c$ and $N = N^*$, then $\dot{N} = 0$ yields $P = h(N^*)$ with $h(N) = \frac{1+N}{m}(1 - \frac{N}{k})$; positivity requires $N^* < k$. \square

Write the predator per-capita growth rate as

$$\psi(N) := \frac{mN}{1+N} - c, \quad \text{so that} \quad \dot{P} = \psi(N) P. \quad (14)$$

Theorem 2.7 (Deterministic predator-prey dynamics) ([Grunert et al. 2021](#); [Cheng 1981](#))
Let $(N(t), P(t))$ solve (5) with $N_0 \in (0, K)$ and $P_0 \in (0, \infty)$. Then we have the following system dynamics:

(i) If $m \leq c$ or $k \leq N^*$, then the critical point K_1 is asymptotically stable and

$$\lim_{t \rightarrow \infty} N(t) = K, \quad \lim_{t \rightarrow \infty} P(t) = 0.$$

(ii) If $N^* < K \leq 1 + 2N^*$, then the critical point K_3 is asymptotically stable and

$$\lim_{t \rightarrow \infty} N(t) = N^*, \quad \lim_{t \rightarrow \infty} P(t) = P^*.$$

(iii) If $K > 1 + 2N^*$, then K_3 is unstable and there exists exactly one periodic orbit in the first quadrant in the (N, P) plane, which is an (asymptotically) stable limit cycle.

Figure 4 shows three dynamic regimes of the deterministic ODE (5).

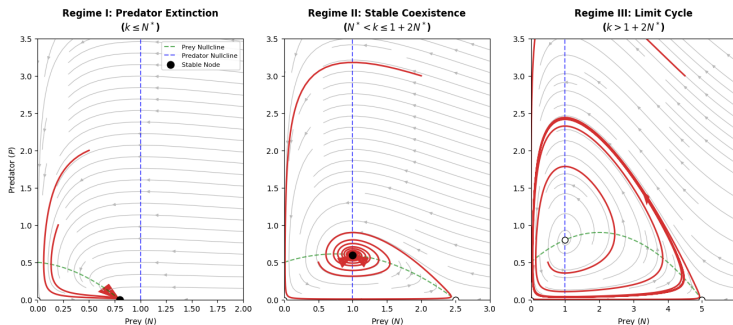


Fig. 4 The three dynamic regimes of the deterministic backbone. Numerical illustration of the stability thresholds detailed in Theorem 2.7. **(Left)** **Regime I:** Low carrying capacity ($k \leq N^*$) leads to predator extinction; trajectories converge to $(k, 0)$. **(Center)** **Regime II:** Intermediate carrying capacity ($N^* < k \leq 1 + 2N^*$) ensures stable coexistence; trajectories spiral into the positive equilibrium K_3 . **(Right)** **Regime III:** High carrying capacity ($k > 1 + 2N^*$) destabilizes K_3 via a Hopf bifurcation, resulting in a stable limit cycle. This transition illustrates the paradox of Enrichment, where increasing resource availability (larger k) induces large-amplitude oscillations.

Remark 2.8 (Dynamics beyond the present scope). The quantity $1 + 2N^*$ is the Hopf bifurcation threshold for k , where the system undergoes bifurcation. When k increases and exceeds $1 + 2N^*$, the interior equilibrium K_3 loses stability and an asymptotically

stable limit cycle emerges, where the predator–prey system manifests as periodically oscillating population cycles. This bifurcation phenomenon facilitates the deterministic Rosenzweig–MacArthur predator–prey model to explain the “paradox of enrichment” (Gounand et al. 2014). Related algebraic–spectral threshold analyses and explicit Hopf onset criteria for Leslie–Gower-type systems have recently been developed, including discrete–continuous stability and bifurcation results (Wang and Yu 2026).

3 Mechanistic event model: a CTMC with absorbing axes

We introduce a mechanistic demographic model at the jump-process level by specifying a CTMC for prey–predator counts. The model is constructed from elementary demographic events (birth, competition, predation/conversion, and death) with state-dependent intensities. This event setting is the input for the system-size scaling and diffusion approximation developed in Sections 4–5.

3.1 State space, event channels, increments, and intensities

Let

$$X(t) = (\mathcal{N}(t), \mathcal{P}(t))^\top \in \mathbb{N}_0^2$$

denote prey and predator counts at time $t \geq 0$. Conditional on the current state $(n, p) \in \mathbb{N}_0^2$, the process experiences one of finitely many elementary events $e \in \mathcal{E} = \{B, C, D, E\}$. Each event has a fixed increment $\Delta_e \in \mathbb{Z}^2$ and an intensity $\Lambda_e(n, p) \geq 0$.

The four event channels are:

Event e	Interpretation	Increment Δ_e	Intensity $\Lambda_e(n, p)$
B	prey birth	$(1, 0)^\top$	n
C	prey competition death	$(-1, 0)^\top$	$\frac{n^2}{k}$
D	predator death	$(0, -1)^\top$	cp
E	predation + conversion	$(-1, 1)^\top$	$\frac{mnp}{1+n}$

Here $k > 0$ is the prey carrying-capacity parameter, $m > 0$ is the maximal predation/conversion rate, and $c > 0$ is the predator mortality rate. The coupled predation/conversion event E changes both coordinates simultaneously and is the source of the negative prey–predator noise covariance in the diffusion approximation (Section 5).

For random time-change representation, let $(Y_e)_{e \in \mathcal{E}}$ be independent unit-rate Poisson processes. Define the event counting processes

$$N_e(t) := Y_e \left(\int_0^t \Lambda_e(X(s)) ds \right), \quad e \in \mathcal{E},$$

so that N_e has predictable intensity $\Lambda_e(X(t))$ with respect to the natural filtration. Then the CTMC admits the exact stochastic integral representation

$$X(t) = X(0) + \sum_{e \in \mathcal{E}} \Delta_e N_e(t), \quad t \geq 0, \quad (15)$$

equivalently, in differential form,

$$dX(t) = \sum_{e \in \mathcal{E}} \Delta_e dN_e(t). \quad (16)$$

Writing components,

$$\begin{aligned} d\mathcal{N}(t) &= dN_B(t) - dN_C(t) - dN_E(t), \\ d\mathcal{P}(t) &= dN_E(t) - dN_D(t). \end{aligned} \quad (17)$$

3.2 Absorbing axes (demographic extinction)

The coordinate axes are absorbing for the CTMC. Indeed, if $\mathcal{N}(t) = 0$ then $\Lambda_B = \Lambda_C = \Lambda_E = 0$, so $\mathcal{N}(s) = 0$ for all $s \geq t$. Similarly, if $\mathcal{P}(t) = 0$ then $\Lambda_D = \Lambda_E = 0$, so $\mathcal{P}(s) = 0$ for all $s \geq t$. Thus demographic extinction at the count level is irreversible.

The event formulation above will be carried through a density-dependent scaling to obtain a diffusion approximation. Because the predation–conversion event E changes prey and predator in opposite directions within the same reaction channel, it induces an instantaneous negative cross-covariance in the diffusion matrix $\Sigma = \sum_e \lambda_e \Delta_e \Delta_e^\top$ (Section 5).

4 System-size scaling and diffusion approximation

The CTMC in Section 3 is formulated at the level of integer counts and therefore carries a natural system-size parameter. Two diffusion-based approximations are commonly employed for Markov chain models: the linear noise approximation (Kampen 1961, 2007) and the chemical Langevin equation (Gillespie 2000, 2002; Kurtz 1978). Linearizing stochastic fluctuations around the deterministic limit derive the linear noise approximation. While this approximation is mathematically well defined for all times, it often evolves outside the positive orthant and may therefore yield nonphysical negative concentration values. Moreover, it is well known that this approach can inadequately represent fluctuations arising from nonlinear reaction rates (Wallace et al. 2012). By contrast, the chemical Langevin equation typically provides a more accurate description in the presence of nonlinearities. However, it is generally only defined up to the first time the process reaches the boundary of the positive orthant. Indeed, because the diffusion coefficients usually contain square roots of molecular concentrations, the unstopped equation becomes ill-posed beyond this point (Manninen et al. 2006; Szpruch and Higham 2010; Wilkie and Wong 2008).

In this work, we adopt the chemical Langevin approach and focus on the system evolution up to the first hitting time of the domain boundary. Our interpretation of the

evolution beyond the first hitting time is freezing the trajectory upon the hitting time, i.e., the trajectory remains where it hits the boundary thereafter. To obtain a diffusion approximation with an explicit noise amplitude and a transparent deterministic limit, we introduce a scaling parameter $\Omega \geq 1$ (effective population size/volume) and work with density variables. The resulting limit falls under the classical density-dependent Markov chain framework of Kurtz (Kurtz 1970, 1971, 1976; Ethier and Kurtz 1986).

For each $\Omega \geq 1$, let $X^\Omega(t) = (\mathcal{N}^\Omega(t), \mathcal{P}^\Omega(t))^\top$ be a CTMC on \mathbb{N}_0^2 with the same event increments Δ_e as in Section 3.1. We define the density (rescaled) process

$$Z^\Omega(t) = (N^\Omega(t), P^\Omega(t))^\top := \Omega^{-1} X^\Omega(t) \in \Omega^{-1} \mathbb{N}_0^2 \subset \mathbb{R}_+^2. \quad (18)$$

Under this scaling, each event changes the density by $\Omega^{-1} \Delta_e$, while the expected number of events over $O(1)$ time intervals is $O(\Omega)$.

For Density-dependent intensities, we choose Ω -dependent intensities of density-dependent form

$$\Lambda_e^\Omega(x) = \Omega \lambda_e(\Omega^{-1} x), \quad x \in \mathbb{N}_0^2, \quad e \in \mathcal{E}, \quad (19)$$

where the rate functions $\lambda_e : \mathbb{R}_+^2 \rightarrow \mathbb{R}_+$ are

$$\lambda_B(N, P) = N, \quad \lambda_C(N, P) = \frac{N^2}{k}, \quad \lambda_D(N, P) = cP, \quad \lambda_E(N, P) = \frac{mNP}{1+N}. \quad (20)$$

With this choice, the random time-change representation in (15) yields

$$Z^\Omega(t) = Z^\Omega(0) + \sum_{e \in \mathcal{E}} \frac{\Delta_e}{\Omega} Y_e \left(\Omega \int_0^t \lambda_e(Z^\Omega(s)) ds \right), \quad (21)$$

where $(Y_e)_{e \in \mathcal{E}}$ are independent unit-rate Poisson processes.

For drift–martingale decomposition and the noise scale. Write $\tilde{Y}_e(u) = Y_e(u) - u$ for the compensated Poisson martingales. Substituting $Y_e(u) = u + \tilde{Y}_e(u)$ into (21) gives the semimartingale decomposition

$$Z^\Omega(t) = Z^\Omega(0) + \int_0^t \mu(Z^\Omega(s)) ds + \rho M^\Omega(t), \quad (22)$$

where the deterministic drift is

$$\mu(z) = \sum_{e \in \mathcal{E}} \Delta_e \lambda_e(z), \quad z \in \mathbb{R}_+^2, \quad (23)$$

and we introduce the canonical demographic noise amplitude

$$\rho = \Omega^{-1/2}. \quad (24)$$

The fluctuation term M^Ω is an \mathbb{R}^2 -valued martingale defined by

$$M^\Omega(t) := \frac{1}{\sqrt{\Omega}} \sum_{e \in \mathcal{E}} \Delta_e \tilde{Y}_e \left(\Omega \int_0^t \lambda_e(Z^\Omega(s)) ds \right). \quad (25)$$

Its predictable quadratic variation is

$$\langle M^\Omega \rangle(t) = \int_0^t \Sigma(Z^\Omega(s)) ds, \quad \Sigma(z) := \sum_{e \in \mathcal{E}} \lambda_e(z) \Delta_e \Delta_e^\top. \quad (26)$$

Thus Σ is $O(1)$ while the prefactor $\rho = \Omega^{-1/2}$ in (22) exhibits the $\Omega^{-1/2}$ fluctuation scale.

For LLN and diffusion limit (informal statement), the following is the canonical limiting picture for density-dependent Markov chains. We state it informally since it is standard; precise hypotheses and proofs can be found in (Kurtz 1970, 1971, 1976; Ethier and Kurtz 1986). The general theme that links stochastic microscale rules to deterministic macroscopic limits also appears in hybrid PDE-ABM settings. Under these settings, mean-field PDE limits are derived from Gillespie-driven agent dynamics (Wang et al. 2025).

Proposition 4.1 (LLN/CLT limits for density-dependent scaling (informal)) *Let Z^Ω be defined by (18)–(21) with rate functions (20). Assume $Z^\Omega(0) \rightarrow z_0 \in \mathbb{R}_+^2$ as $\Omega \rightarrow \infty$.*

(LLN) *Z^Ω converges in probability, uniformly on compact time intervals, to the unique solution $z(\cdot)$ of the mean-field ODE*

$$\dot{z}(t) = \mu(z(t)), \quad z(0) = z_0. \quad (27)$$

(CLT) *The fluctuation process $\sqrt{\Omega}(Z^\Omega - z)$ converges in distribution (in the Skorokhod topology) to an Itô diffusion whose drift is given by the linearization of μ along $z(t)$ and whose instantaneous covariance is $\Sigma(z(t))$.*

Remark 4.2 (Connection to chemical Langevin and reaction-channel form). The covariance representation (26) coincides with the standard reaction-channel covariance formula used in chemical Langevin approximations and stochastic reaction network theory (Gillespie 1977, 2000; Kampen 2007; Anderson and Kurtz 2011). In particular, coupled events that simultaneously change multiple coordinates (here, predation–conversion) induce off-diagonal covariance terms in the diffusion limit.

5 Limiting drift and covariance; mechanistic negative correlation

In this section we compute the limiting drift and instantaneous covariance implied by the mechanistic event model of Section 3 under the density-dependent scaling of Section 4. The off-diagonal entry $\Sigma_{12} < 0$ will emerge as a direct mechanistic

fingerprint of the coupled predation–conversion channel: a single event decreases prey while (with conversion) increasing predators.

Explicit drift and diffusion matrix. Let λ_e be the density-level event rates in (20) and let $\Delta_e \in \mathbb{Z}^2$ denote the event increments from Section 3.1. Recall the definitions

$$\mu(z) = \sum_{e \in \mathcal{E}} \Delta_e \lambda_e(z), \quad \Sigma(z) = \sum_{e \in \mathcal{E}} \lambda_e(z) \Delta_e \Delta_e^\top, \quad z = (N, P) \in \mathbb{R}_+^2. \quad (28)$$

With the conventions

$$\Delta_B = \begin{pmatrix} 1 \\ 0 \end{pmatrix}, \quad \Delta_C = \begin{pmatrix} -1 \\ 0 \end{pmatrix}, \quad \Delta_D = \begin{pmatrix} 0 \\ -1 \end{pmatrix}, \quad \Delta_E = \begin{pmatrix} -1 \\ 1 \end{pmatrix},$$

and with the rates (20), we obtain the explicit drift

$$\mu(N, P) = \begin{pmatrix} N - \frac{N^2}{k} - \frac{mNP}{1+N} \\ \frac{mNP}{1+N} - cP \end{pmatrix} \quad (29)$$

which coincides with the Rosenzweig–MacArthur vector field in (5). Moreover, the diffusion (instantaneous covariance) matrix is

$$\Sigma(N, P) = \begin{pmatrix} N + \frac{N^2}{k} + \frac{mNP}{1+N} & -\frac{mNP}{1+N} \\ -\frac{mNP}{1+N} & cP + \frac{mNP}{1+N} \end{pmatrix}. \quad (30)$$

In particular, for $(N, P) \in U = (0, \infty)^2$ one has the strict mechanistic negative correlation

$$\Sigma_{12}(N, P) = -\frac{mNP}{1+N} < 0. \quad (31)$$

Event-based Brownian factorization, it is often convenient to encode (30) by an “event matrix” that preserves the mechanistic decomposition by reaction channels. Define

$$L_{\text{ev}}(N, P) := \left[\sqrt{\lambda_B(N, P)} \Delta_B, \sqrt{\lambda_C(N, P)} \Delta_C, \sqrt{\lambda_D(N, P)} \Delta_D, \sqrt{\lambda_E(N, P)} \Delta_E \right] \in \mathbb{R}^{2 \times 4}, \quad (32)$$

where λ_e are as in (20). Writing columns explicitly,

$$L_{\text{ev}}(N, P) = \begin{pmatrix} \sqrt{N} & -\sqrt{\frac{N^2}{k}} & 0 & -\sqrt{\frac{mNP}{1+N}} \\ 0 & 0 & -\sqrt{cP} & \sqrt{\frac{mNP}{1+N}} \end{pmatrix}. \quad (33)$$

Lemma 5.1 (Event factorization) *For all $(N, P) \in \mathbb{R}_+^2$,*

$$\Sigma(N, P) = L_{\text{ev}}(N, P) L_{\text{ev}}(N, P)^\top. \quad (34)$$

Consequently, if $W(t) = (W_B(t), W_C(t), W_D(t), W_E(t))^\top$ is a standard \mathbb{R}^4 Brownian motion, then the diffusion approximation associated with (29)–(30) can be written in reaction-channel (event) form as

$$dZ(t) = \mu(Z(t)) dt + \rho L_{\text{ev}}(Z(t)) dW(t), \quad \rho = \Omega^{-1/2}, \quad (35)$$

whenever the path remains in $U = (0, \infty)^2$.

Proof By definition (32),

$$\begin{aligned} L_{\text{ev}}(N, P) L_{\text{ev}}(N, P)^\top &= \sum_{e \in \mathcal{E}} (\sqrt{\lambda_e(N, P)} \Delta_e) (\sqrt{\lambda_e(N, P)} \Delta_e)^\top \\ &= \sum_{e \in \mathcal{E}} \lambda_e(N, P) \Delta_e \Delta_e^\top = \Sigma(N, P), \end{aligned}$$

which is (34). The SDE representation (35) follows from the standard identification of a diffusion with covariance Σ via any factor L such that $\Sigma = LL^\top$. \square

The factor L_{ev} preserves the mechanistic decomposition by event channels and is therefore natural for both analysis and simulation. Since there are four reaction channels, L_{ev} is 2×4 and the driving Brownian motion in (35) is 4-dimensional. In Section 5 we record a two-dimensional (Cholesky) factorization on U that is sometimes preferable for computation.

Positive definiteness on the interior and degeneracy on the boundary. The diffusion matrix (30) is uniformly nondegenerate on compact subsets of the interior U , while it degenerates on the axes where one or more event rates vanish.

Lemma 5.2 (Positive definiteness on the interior; boundary degeneracy) *For all $(N, P) \in (0, \infty)^2$, the matrix $\Sigma(N, P)$ in (30) is symmetric and positive definite. On the boundary $\partial U = \{N = 0\} \cup \{P = 0\}$ it is positive semidefinite and may be singular (degenerate).*

Proof Symmetry is immediate from (30). For $N > 0$ and $P > 0$ we have

$$\Sigma_{11}(N, P) = N + \frac{N^2}{k} + \frac{mNP}{1+N} > 0, \quad \Sigma_{22}(N, P) = cP + \frac{mNP}{1+N} > 0.$$

Moreover,

$$\begin{aligned} \det \Sigma(N, P) &= \left(N + \frac{N^2}{k} + \frac{mNP}{1+N} \right) \left(cP + \frac{mNP}{1+N} \right) - \left(\frac{mNP}{1+N} \right)^2 \\ &= \left(N + \frac{N^2}{k} \right) \left(cP + \frac{mNP}{1+N} \right) + \frac{mNP}{1+N} cP > 0. \end{aligned}$$

Thus $\Sigma(N, P)$ has positive trace and positive determinant, hence is positive definite on $(0, \infty)^2$.

If $N = 0$ or $P = 0$, then one or more rates in (20) vanish and (30) shows that Σ is positive semidefinite but generally singular. For example,

$$\Sigma(0, P) = \begin{pmatrix} 0 & 0 \\ 0 & cP \end{pmatrix}, \quad \Sigma(N, 0) = \begin{pmatrix} N + \frac{N^2}{k} & 0 \\ 0 & 0 \end{pmatrix},$$

so degeneracy occurs on each axis. \square

By continuity of Σ and Lemma 5.2, for every compact $K \Subset U$ there exists $\lambda_K > 0$ such that $\xi^\top \Sigma(z)\xi \geq \lambda_K |\xi|^2$ for all $z \in K$ and $\xi \in \mathbb{R}^2$.

Cholesky factorization (two-dimensional Brownian driver)

For analysis and simulation it is sometimes preferable to drive the diffusion by a two-dimensional Brownian motion. On the interior $U = (0, \infty)^2$, this can be achieved by any matrix square root of Σ , for instance the unique Cholesky factor with positive diagonal entries.

By Lemma 5.2, for $(N, P) \in U$ there exists a unique lower-triangular matrix $L_{\text{chol}}(N, P) \in \mathbb{R}^{2 \times 2}$ with positive diagonal entries such that

$$\Sigma(N, P) = L_{\text{chol}}(N, P) L_{\text{chol}}(N, P)^\top. \quad (36)$$

An explicit choice is

$$L_{\text{chol}}(N, P) = \begin{pmatrix} \sqrt{\Sigma_{11}(N, P)} & 0 \\ \frac{\Sigma_{21}(N, P)}{\sqrt{\Sigma_{11}(N, P)}} & \sqrt{\Sigma_{22}(N, P) - \frac{\Sigma_{21}(N, P)^2}{\Sigma_{11}(N, P)}} \end{pmatrix}, \quad (37)$$

where Σ_{ij} are the entries in (30). In particular, the second diagonal entry is well-defined and strictly positive on U because Σ is positive definite there.

Hence, if $B(t)$ is a standard \mathbb{R}^2 Brownian motion, the same diffusion approximation can be written as

$$dZ(t) = \mu(Z(t)) dt + \rho L_{\text{chol}}(Z(t)) dB(t), \quad \rho = \Omega^{-1/2}, \quad (38)$$

whenever the path remains in U .

Equations (35) and (38) define the same diffusion on U since both factors satisfy $LL^\top = \Sigma$ on the interior. The event factorization preserves reaction-channel structure and is natural from the mechanistic standpoint, while the Cholesky factorization reduces the driving noise dimension and is often convenient for computation. In Section 8 we include finite-sample diagnostics illustrating the consistency of these two implementations under an absorbed discretization scheme.

Remark 5.3 (Mechanistic fingerprint: negative demographic noise correlation). The strict negativity of the cross-covariance

$$\Sigma_{12}(N, P) = -\frac{mNP}{1+N} < 0 \quad \text{on } U$$

is a direct structural consequence of the underlying event setting. It serves as a clear fingerprint distinguishing this diffusion from ad hoc diagonal-noise models. Specifically, the predation-conversion channel E has increment $\Delta_E = (-1, 1)^\top$, reflecting the simultaneous loss of one prey and gain of one predator. In the density-dependent diffusion limit, each channel contributes $\lambda_e \Delta_e \Delta_e^\top$ to the instantaneous covariance. For E ,

$$\lambda_E(N, P) \Delta_E \Delta_E^\top = \frac{mNP}{1+N} \begin{pmatrix} 1 & -1 \\ -1 & 1 \end{pmatrix},$$

whose off-diagonal entries are strictly negative whenever both species are present. By contrast, diagonal-noise SDEs enforce $\Sigma_{12} \equiv 0$ and therefore cannot capture this event-level coupling. Thus, the sign and magnitude of Σ_{12} encode a mechanistic constraint rather than an imposed correlation structure.

6 Full-covariance diffusion with absorption: definition and basic properties

We now define the diffusion approximation on the interior $U = (0, \infty)^2$ using the mechanistic drift μ and covariance Σ from Section 5, and we impose absorption at the axes by freezing the process upon first hitting $\partial U = \{N = 0\} \cup \{P = 0\}$. This absorbed convention mirrors the irreversibility of demographic extinction in the underlying CTMC.

Throughout this section we work on a filtered probability space $(\Omega, \mathcal{F}, (\mathcal{F}_t)_{t \geq 0}, \mathbb{P})$ satisfying the usual conditions. Let $U := (0, \infty)^2$ and $\bar{U} := [0, \infty)^2$. We fix parameters $k > 0$, $m > 0$, $c > 0$, and a noise scale $\rho > 0$.

Let $\mu : \bar{U} \rightarrow \mathbb{R}^2$ and $\Sigma : \bar{U} \rightarrow \mathbb{R}^{2 \times 2}$ be given by (29)–(30). On U we use the event-based factor $L_{\text{ev}} : \bar{U} \rightarrow \mathbb{R}^{2 \times 4}$ defined in (33), so that $\Sigma(z) = L_{\text{ev}}(z) L_{\text{ev}}(z)^\top$ for all $z \in \bar{U}$ (Lemma 5.1).

Definition 6.1 (Interior SDE and absorption time). Let $z_0 = (N_0, P_0) \in U$ and let $W = (W_1, \dots, W_4)^\top$ be a standard \mathbb{R}^4 Brownian motion. An interior strong solution starting from z_0 is an U -valued, continuous, adapted process $Z(t) = (N(t), P(t))$ defined up to a (possibly infinite) stopping time τ such that

$$Z(t) = z_0 + \int_0^{t \wedge \tau} \mu(Z(s)) ds + \rho \int_0^{t \wedge \tau} L_{\text{ev}}(Z(s)) dW(s), \quad t \geq 0, \quad (39)$$

and such that

$$\tau := \inf\{t > 0 : Z(t) \notin U\} = \inf\{t > 0 : N(t) = 0 \text{ or } P(t) = 0\}. \quad (40)$$

Definition 6.2 (Absorbed extension). Given an interior strong solution (Z, τ) as in Definition 6.1, the absorbed process \hat{Z} is defined for all $t \geq 0$ by

$$\hat{Z}(t) := \begin{cases} Z(t), & t < \tau, \\ Z(\tau), & t \geq \tau. \end{cases} \quad (41)$$

We refer to τ as the absorption time.

The freezing rule (41) encodes demographic extinction: once a coordinate reaches 0, the corresponding species is considered extinct and the process remains at the boundary thereafter (Figure 5). We illustrate one set of representative time evolution of the absorbed process in Figure 6. This convention is consistent with the CTMC model (Section 3.2), where the axes are absorbing because birth or predation events are impossible in the absence of individuals.

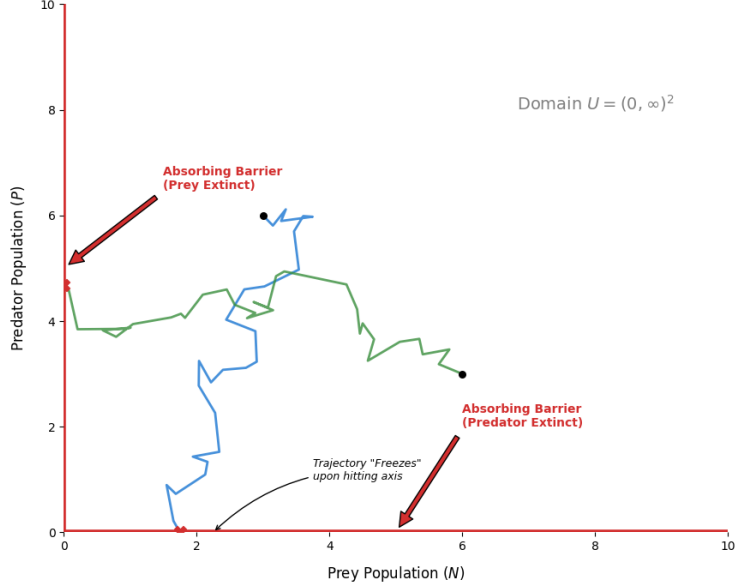


Fig. 5 Absorption rule. The model treats extinction as irreversible. Once a trajectory hits either axis ($N = 0$ or $P = 0$), the diffusion is frozen (marked by 'X'), representing the demographic end of a species.

Strong existence and pathwise uniqueness up to absorption. This subsection proves that the interior SDE (39) is strongly well-posed up to the absorption time τ and that the absorbed extension (41) is well-defined. The argument is a standard localization construction based on truncated globally Lipschitz coefficients; see, e.g., (Karatzas and Shreve 1998; Ikeda and Watanabe 1981; Øksendal 2003).

We now present a fully explicit truncation map and give a detailed localization proof that will be convenient to cite later. For the SDE (35), the drift vector and the volatility matrix are locally Lipschitz continuous on U . Local Lipschitz continuity ensures local well-posedness.

Theorem 6.3 (Strong well-posedness up to absorption) (Karatzas and Shreve 1998) *Fix $z_0 \in U$ and let W be a standard \mathbb{R}^4 Brownian motion. Consider the interior SDE*

$$dZ(t) = \mu(Z(t)) dt + \rho L_{\text{ev}}(Z(t)) dW(t), \quad Z(0) = z_0, \quad (42)$$

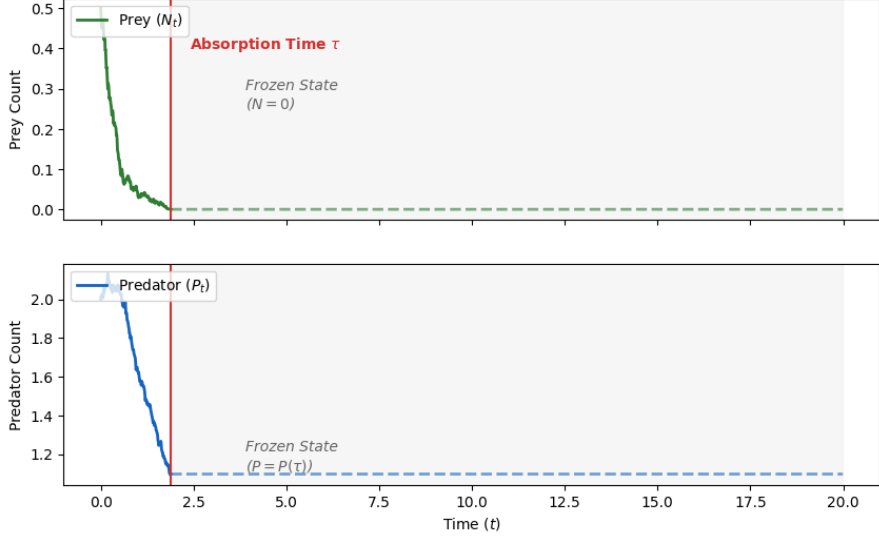


Fig. 6 Time evolution of the absorbed process $\hat{Z}(t)$. Simulation of a single stochastic trajectory illustrates the freezing convention in Definition 6.2. The vertical red line marks the absorption time τ when the prey population (N_t , green) hits zero. For all times $t \geq \tau$ (gray shaded region), the entire state vector is frozen at $Z(\tau)$. Note that the predator count (P_t , blue) does not decay to zero but remains constant at its value at the moment of prey extinction ($P(\tau)$). This definition formalizes the irreversibility of extinction for the stopped SDE analysis.

with absorption time $\tau = \inf\{t > 0 : Z(t) \notin U\}$. Then there exists an (\mathcal{F}_t) -adapted continuous process Z defined on $[0, \tau)$ such that (42) holds on $[0, \tau)$, and Z is a strong solution in the sense that for each $t < \tau$, $Z(t)$ is measurable with respect to $\sigma(z_0, W(s) : 0 \leq s \leq t)$. Moreover, pathwise uniqueness holds on $[0, \tau)$: if $Z^{(1)}$ and $Z^{(2)}$ are two solutions driven by the same Brownian motion W with the same initial condition z_0 , then

$$\mathbb{P}(Z^{(1)}(t) = Z^{(2)}(t) \text{ for all } t < \tau^{(1)} \wedge \tau^{(2)}) = 1.$$

In particular, the absorbed extension \hat{Z} defined by (41) is well-defined and unique in law.

Non-explosion and moment bounds, we record a quadratic Lyapunov estimate for the interior SDE (42), which yields non-explosion prior to absorption and uniform polynomial-moment bounds on finite time horizons. Throughout, write $Z = (N, P)$ and denote by $\Sigma(z) := L_{\text{ev}}(z)L_{\text{ev}}(z)^\top$ the covariance matrix on U , cf. Section 5. Let \mathcal{L} be the (interior) generator

$$(\mathcal{L}f)(z) = \langle \mu(z), \nabla f(z) \rangle + \frac{\rho^2}{2} \text{Tr}(\Sigma(z) \nabla^2 f(z)), \quad z \in U, \quad (43)$$

for $f \in C^2(U)$.

Theorem 6.4 (Non-explosion and polynomial moment bound) *Let $z_0 \in U$ and let Z be the unique strong solution on $[0, \tau)$ from Theorem 6.3. Define the radial exit times*

$$\sigma_R := \inf\{t \geq 0 : |Z(t)| \geq R\}, \quad R \geq 1,$$

and the associated explosion time $\zeta := \lim_{R \rightarrow \infty} \sigma_R \in (0, \infty]$. Then:

- (i) *(Non-explosion) One has $\mathbb{P}(\zeta = \infty) = 1$. In particular, the maximal lifetime of the interior SDE is τ , i.e., there is no blow-up prior to hitting ∂U .*
- (ii) *(Polynomial moment bound) Assume either $p = 2$ or $p \geq 4$. Fix $T > 0$. There exists a constant $C_{p,T} < \infty$ depending only on (k, m, c, ρ, p) and T such that for every initial condition $z_0 \in U$,*

$$\sup_{0 \leq t \leq T} \mathbb{E}[|Z(t \wedge \tau)|^p] \leq C_{p,T}(1 + |z_0|^p). \quad (44)$$

For completeness, details are provided in Appendix A. Related population models also establish global well-posedness by explicit moment bounds (Liang et al. 2025).

7 Boundary structure and extinction results

This section collects qualitative results on extinction for the absorbed diffusion introduced in Section 6. We emphasize two complementary viewpoints. The first is the absorbed dynamics, in which trajectories are frozen upon reaching the axes and extinction is irreversible. The second is an optional model completion along the boundary, used only for ecological interpretation of post-extinction dynamics of the remaining species.

Absorbing axes and reduced boundary dynamics (optional completion). Recall the open quadrant $U := (0, \infty)^2$ and the absorption time

$$\tau := \inf\{t \geq 0 : Z(t) \in \partial U\}, \quad \partial U = (\{0\} \times [0, \infty)) \cup ([0, \infty) \times \{0\}), \quad (45)$$

for the interior diffusion $Z(t) = (N(t), P(t))^\top$ constructed in Section 6. We write \widehat{Z} for the absorbed extension (frozen after τ), as in Definition 6.2.

Proposition 7.1 (Absorbing axes for the frozen extension) *Let \widehat{Z} be the absorbed process defined by $\widehat{Z}(t) = Z(t)$ for $t < \tau$ and $\widehat{Z}(t) = Z(\tau)$ for $t \geq \tau$. Then ∂U is absorbing for \widehat{Z} : if $\widehat{Z}(t_0) \in \partial U$ for some $t_0 \geq 0$, then $\widehat{Z}(t) \equiv \widehat{Z}(t_0)$ for all $t \geq t_0$. In particular, the coordinate axes represent irreversible extinction events in the absorbed model.*

For ecological interpretation it is sometimes convenient to continue the dynamics after one species has gone extinct, letting the remaining species evolve according to the corresponding one-dimensional diffusion obtained by restricting the coefficients to the boundary. This completion is not used in the extinction proofs below (which are formulated for the absorbed process), and it is introduced only as an auxiliary model component.

Definition 7.2 (Axis-restricted diffusions). Let $\rho > 0$ be the demographic noise amplitude. Define the prey-axis and predator-axis coefficients by restriction:

$$\mu_N(N, 0) = N - \frac{N^2}{k}, \quad \Sigma_{11}(N, 0) = N + \frac{N^2}{k}, \quad N \geq 0,$$

and

$$\mu_P(0, P) = -cP, \quad \Sigma_{22}(0, P) = cP, \quad P \geq 0.$$

The prey-axis diffusion $N^{(0)}$ is the one-dimensional SDE on $[0, \infty)$

$$dN^{(0)}(t) = \left(N^{(0)}(t) - \frac{(N^{(0)}(t))^2}{k} \right) dt + \rho \sqrt{N^{(0)}(t) + \frac{(N^{(0)}(t))^2}{k}} dB_1(t), \quad (46)$$

and the predator-axis diffusion $P^{(0)}$ is the one-dimensional SDE on $[0, \infty)$

$$dP^{(0)}(t) = -cP^{(0)}(t) dt + \rho \sqrt{cP^{(0)}(t)} dB_2(t). \quad (47)$$

Here, B_1, B_2 are standard one-dimensional Brownian motions (independent, unless specified otherwise).

Lemma 7.3 (Well-posedness on the axes) *For any initial condition $N^{(0)}(0) \geq 0$ (resp. $P^{(0)}(0) \geq 0$), the SDE (46) (resp. (47)) admits a pathwise unique strong solution with values in $[0, \infty)$. Moreover, 0 is absorbing for both axis-restricted diffusions.*

Proof For (47) this is the classical Cox–Ingersoll–Ross (CIR) square-root diffusion with linear drift, for which strong existence and uniqueness are standard; see, e.g., (Karatzas and Shreve 1998; Revuz and Yor 1999). Since both drift and diffusion vanish at 0, the boundary point 0 is absorbing. The invariance of $[0, \infty)$ follows.

For (46), the drift is locally Lipschitz and the diffusion coefficient $x \mapsto \sqrt{x + x^2/k}$ is Hölder-1/2 and of linear growth on $[0, \infty)$. Standard one-dimensional criteria (e.g. Yamada–Watanabe-type results for Hölder-1/2 diffusion coefficients) yield strong existence/uniqueness and nonnegativity. We refer to (Jeanblanc et al. 2009; Revuz and Yor 1999) for these results. Absorption at 0 follows since both drift and diffusion vanish at 0. \square

Positive probability of extinction for all parameters. We next prove that, regardless of parameters, extinction occurs with strictly positive probability starting from any interior state. Recall the absorption time $\tau = \inf\{t \geq 0 : Z(t) \in \partial U\}$ from (40). Throughout, Z denotes the unique strong solution on $[0, \tau)$ from Theorem 6.3, and \widehat{Z} denotes the absorbed extension.

Theorem 7.4 (Positive extinction probability) *Assume $k > 0$, $m > 0$, $c > 0$ and $\rho > 0$. Then for every initial condition $z = (N_0, P_0) \in U$,*

$$\mathbb{P}_z(\tau < \infty) > 0. \quad (48)$$

Equivalently, $\mathbb{P}_z(\widehat{Z}(t) \in \partial U \text{ for some } t \geq 0) > 0$ for all $z \in U$.

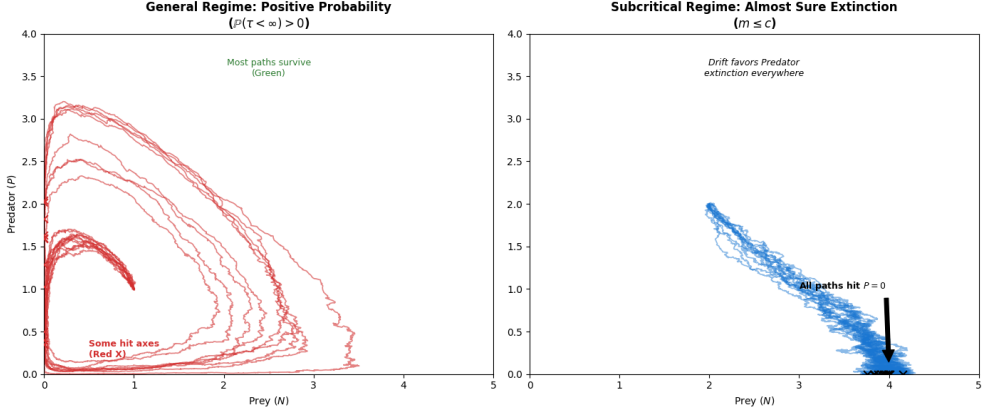


Fig. 7 Stochastic extinction scenarios: positive probability vs. almost sure extinction. Numerical illustration of the main results in Section 7. **(Left)** In the general regime (Theorem 7.4), even if the deterministic system predicts coexistence (limit cycles), stochastic fluctuations drive a fraction of paths to extinction (red trajectories marked with 'X'), while others survive transiently (green labels). Extinction is possible but not guaranteed. **(Right)** In the subcritical regime $m \leq c$ (Theorem 7.5), the predator goes extinct eventually. The drift is uniformly non-positive for the predator, forcing almost sure extinction (all blue paths hit the axis $P = 0$) regardless of initial conditions.

For completeness, we include a self-contained proof in Appendix B.

Almost sure predator extinction in the subcritical regime. We now identify a parameter regime in which predator extinction occurs almost surely. The key assumption is that the maximal per-capita predator growth rate does not overcome baseline mortality:

$$m \leq c. \quad (49)$$

In this regime, the predator has nonpositive drift throughout the interior, and the square-root demographic noise remains active down to the boundary, forcing eventual absorption at $P = 0$.

Theorem 7.5 (Almost sure predator extinction in the subcritical regime) *Assume (49). Then for every initial condition $z = (N_0, P_0) \in U$, the predator component of the interior diffusion satisfies*

$$\mathbb{P}_z \left(\inf \{t \geq 0 : P(t) = 0\} < \infty \right) = 1. \quad (50)$$

Consequently, $\mathbb{P}_z(\tau < \infty) = 1$ and the absorbed process \hat{Z} satisfies $\hat{Z}(t) \in \partial U$ for all sufficiently large t , almost surely.

For completeness, we include a self-contained proof in Appendix C. Figure 7 compares two stochastic extinction scenarios presented in Theorems 7.4–7.5.

8 Numerical methods and diagnostics

This section documents the numerical procedures used to illustrate and corroborate the qualitative statements proved in Sections 3–7.

8.1 Deterministic check

We include a minimal deterministic sanity check for the Rosenzweig–MacArthur ODE (5), used in this paper only for parameter interpretation and as a qualitative reference for bounded coexistence versus deterministic extinction. All simulations in this subsection use a standard adaptive Runge–Kutta solver (RK45) with strict tolerances, and only serve as brief consistency checks. We do not pursue detailed deterministic bifurcation computations in this work. Throughout this numerical check we fix $(m, c, k) = (2.0, 0.8, 3.0)$ and integrate (5) from three interior initial conditions.

Since $m > c$ and

$$N^* = \frac{c}{m - c} = \frac{0.8}{2.0 - 0.8} = \frac{2}{3} \approx 0.6667, \quad k = 3.0 > N^*,$$

the coexistence equilibrium $K_3 = (N^*, P^*)$ exists (Proposition 2.6), with

$$P^* = \frac{1 + N^*}{m} \left(1 - \frac{N^*}{k}\right) \approx 0.6481, \quad \text{so that} \quad K_3 \approx (0.6667, 0.6481).$$

For the same parameters, the Hopf threshold for the trace of the linearization at K_3 is $k_H = 1 + 2N^* \approx 2.3333$ (cf. Remark 2.8 in the deterministic analysis). Because $k = 3.0 > k_H$, the Jacobian trace at K_3 is positive (numerically $\text{tr } J(K_3) \approx 8.89 \times 10^{-2}$), so K_3 is unstable. Consistent with the local diagnosis, Figure 8 shows that trajectories initialized in U exhibit sustained oscillations on the simulated time window and approach a closed orbit in the phase plane.

As a separate sanity check of the deterministic extinction condition, we simulate an example with $m \leq c$: $(m, c, k) = (0.8, 0.8, 1.0)$. In this subcritical regime, Theorem 2.7 predicts $P(t) \rightarrow 0$ and $N(t) \rightarrow k$ for $N_0 > 0$, which is confirmed numerically (at $t = 200$ we observe $N \approx 1.0$ and $P \approx 0.0$ up to solver tolerance).

8.2 Stochastic simulation of the absorbed mechanistic diffusion

We simulate the mechanistic full-covariance diffusion approximation on $U = (0, \infty)^2$,

$$dZ(t) = \mu(Z(t)) dt + \rho L(Z(t)) dB(t), \quad Z(0) = z \in U, \quad (51)$$

with drift μ and covariance $\Sigma = LL^\top$ given by (29)–(30). Unless stated otherwise, we fix the noise amplitude at $\rho = \Omega^{-1/2} = 0.1$ (corresponding to $\Omega = 100$), and parameters $(k, m, c) = (3.0, 2.0, 0.8)$ in the super-Hopf coexistence setting. All simulations use the absorbed convention of Section 6: once a coordinate hits 0, the process is frozen on the boundary. This is the diffusion-level analogue of demographic irreversibility in the CTMC (Section 3.2).

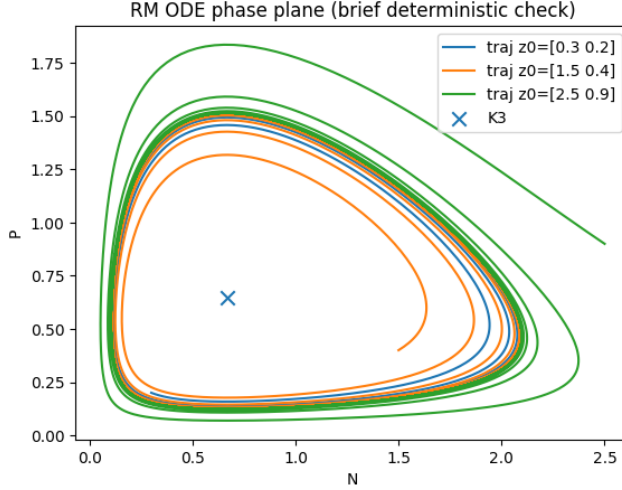


Fig. 8 Representative trajectories when the coexistence equilibrium exists with the asymptotically stable limit cycle.

We employ the EM scheme with time step Δt :

$$Z_{n+1} = Z_n + \mu(Z_n)\Delta t + \rho L(Z_n) \Delta B_n, \quad \Delta B_n \sim \mathcal{N}(0, \Delta t I), \quad (52)$$

where $Z_n \approx Z(n\Delta t)$ and the dimension of the Gaussian increment ΔB_n matches the chosen factor L (event factorization: 4D; Cholesky factorization: 2D).

Since the target continuous-time model is absorbed at ∂U and then frozen, we enforce absorption at the discrete level by the following clipping+freezing rule. Define the discrete absorption time

$$\tau_{\Delta t} := \inf\{n\Delta t : (Z_n)_1 \leq 0 \text{ or } (Z_n)_2 \leq 0\}.$$

At the first step where a component becomes nonpositive, we clip componentwise,

$$(Z_{n+1})_i \leftarrow \max\{(Z_{n+1})_i, 0\}, \quad i = 1, 2,$$

and for all subsequent steps we freeze,

$$Z_{n+1} = Z_n \quad \text{for all } n\Delta t \geq \tau_{\Delta t}.$$

This absorption treatment is a numerical implementation of the demographic extinction convention: once prey or predator density reaches 0, the corresponding species is extinct and the state remains on the boundary thereafter.

We implement (51) using either the event-based factorization $L = L_{\text{ev}} \in \mathbb{R}^{2 \times 4}$ (33), or the Cholesky factorization $L = L_{\text{chol}} \in \mathbb{R}^{2 \times 2}$ (37). Figure 9 shows representative absorbed EM trajectories under both factorizations. In the Cholesky-based sample path, the prey component crosses $N = 0$ boundary, triggering absorption on the finite

simulation window. Accordingly, the discrete absorption time is $\tau_{\Delta t} = 87.78$ for the particular realization. In contrast, the event-based sample path predicts the extinction of the predator population with $\tau_{\Delta t} = 51.31$. The extinction of either population is consistent with the model. The theory establishes a positive extinction probability in the general parameter regime (Theorem 7.4), so absorption on a finite horizon occurs with positive probability.

To summarize extinction events statistically, we compute the survival curve $t \mapsto \mathbb{P}(\tau_{\Delta t} > t)$ by Monte Carlo sampling. Figure 10 reports an estimate based on $M = 1000$ independent absorbed EM paths (Cholesky factorization, $\Delta t = 10^{-2}$, $T = 100$). The resulting decay of the survival probability over the simulation window provides a direct numerical diagnostic of extinction-by-absorption under demographic noise, complementing the qualitative statement of Theorem 7.4.

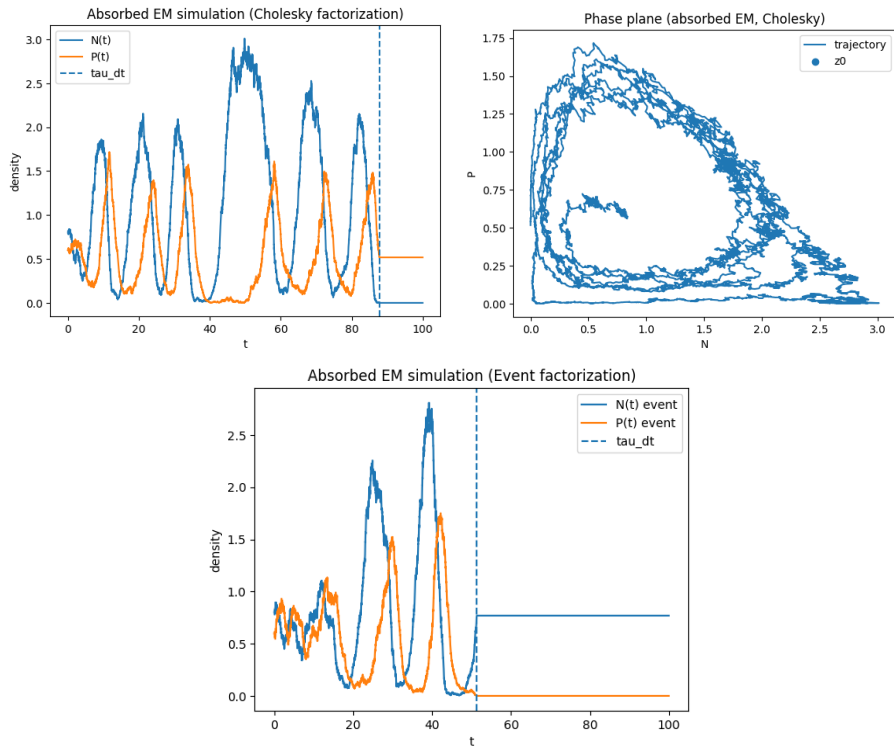


Fig. 9 Absorbed Euler–Maruyama (EM) simulation (illustrative paths). Representative absorbed EM trajectories for the mechanistic diffusion (51) using (top two) the Cholesky factorization L_{chol} and (bottom) the event factorization L_{ev} . Absorption is enforced by clipping at the first non-positive coordinate and freezing thereafter. Parameters: $(k, m, c) = (3.0, 2.0, 0.8)$, $\rho = 0.1$ ($\Omega = 100$), $\Delta t = 10^{-2}$, $T = 100$, $z_0 = (0.8, 0.6)$. In the displayed single-path realizations, $\tau_{\Delta t} = 87.78$ and $\tau_{\Delta t} = 51.31$ on $[0, T]$ for the Cholesky-based and event-based sample path.

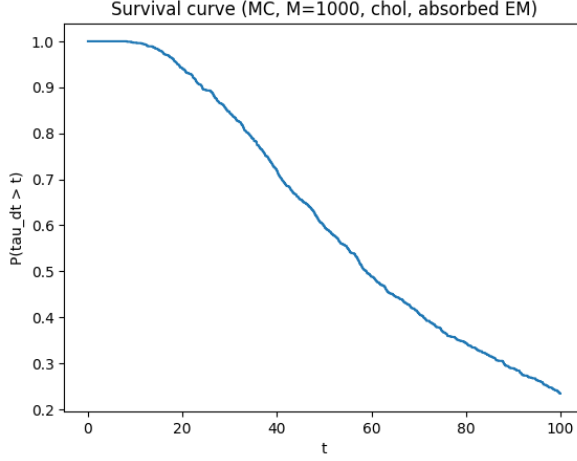


Fig. 10 Survival curve under absorbed EM (Monte Carlo). Monte Carlo estimate of $t \mapsto \mathbb{P}(\tau_{\Delta t} > t)$ based on $M = 1000$ absorbed EM paths (Cholesky factorization). Parameters: $(k, m, c) = (3.0, 2.0, 0.8)$, $\rho = 0.1$, $\Delta t = 10^{-2}$, $T = 50$, $z_0 = (0.8, 0.6)$. The decay over the simulated horizon provides a finite-resolution diagnostic of extinction-by-absorption.

8.3 Factorization consistency (event versus Cholesky)

On the interior U , both the event-based factorization $L_{\text{ev}} \in \mathbb{R}^{2 \times 4}$ (33) and the Cholesky factorization $L_{\text{chol}} \in \mathbb{R}^{2 \times 2}$ (37) satisfy

$$L_{\text{ev}}(z)L_{\text{ev}}(z)^\top = \Sigma(z) = L_{\text{chol}}(z)L_{\text{chol}}(z)^\top, \quad z \in U,$$

and therefore represent the same diffusion in continuous time. Our implementation uses a time discretization and an absorbed stopping rule at ∂U (Section 8.2). Therefore, it is important to verify that the two factorizations yield consistent finite-resolution statistics at the numerical settings used in this paper.

We compare absorbed EM simulations (52) using $L = L_{\text{ev}}$ (4D Brownian driver) and $aL = L_{\text{chol}}$ (2D Brownian driver), under identical model parameters and discretization:

$$(k, m, c) = (3.0, 2.0, 0.8), \quad \rho = 0.1 (\Omega = 100), \quad \Delta t = 10^{-2}, \quad T = 100, \quad z_0 = (0.8, 0.6).$$

For each factorization we generate $M = 2000$ independent absorbed EM paths (with independent random seeds across the two implementations).

We report three diagnostics that are directly tied to models:

- (i) Unconditional mean trajectories. Empirical averages $t \mapsto \widehat{\mathbb{E}}[N(t)]$ and $t \mapsto \widehat{\mathbb{E}}[P(t)]$.
- (ii) Survival curves. Empirical survival probabilities $t \mapsto \widehat{\mathbb{P}}(\tau_{\Delta t} > t)$, where $\tau_{\Delta t}$ is the discrete absorption time defined in Section 8.2.

(iii) Conditional marginal at T . The empirical distribution of $N(T)$ conditioned on survival $\{\tau_{\Delta t} > T\}$.

Figure 11 displays the results. The empirical mean trajectories under the two factorizations are visually indistinguishable at the plotted resolution (left panel), and the survival curves track each other closely over $[0, T]$ (middle panel). At the terminal time $T = 100$, the estimated survivor fractions are

$$\widehat{\mathbb{P}}(\tau_{\Delta t} > T) = 0.244 \quad (\text{event factorization}), \quad \widehat{\mathbb{P}}(\tau_{\Delta t} > T) = 0.245 \quad (\text{Cholesky factorization}),$$

a difference of 0.41% in survival probability at this finite Monte Carlo resolution. Such discrepancies are expected under independent Monte Carlo sampling across methods and the non-smooth absorbed discretization (clipping+freezing). Finally, the conditional histograms of $N(T)$ given survival overlap closely (right panel), indicating no visible factorization-induced bias in the survival-conditioned distribution at this resolution.

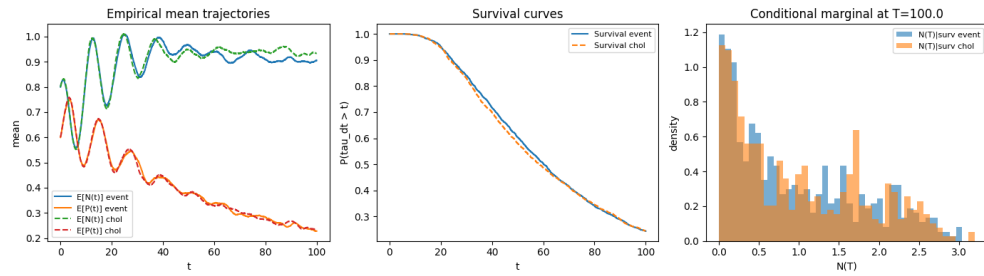


Fig. 11 Finite-sample consistency of diffusion factorizations. Monte Carlo comparison of absorbed EM simulations using the event-based factorization (L_{ev} , 4D noise) and the Cholesky factorization (L_{chol} , 2D noise), both satisfying $LL^{\top} = \Sigma$ on U . **Left:** empirical mean trajectories $\widehat{\mathbb{E}}[N(t)]$ and $\widehat{\mathbb{E}}[P(t)]$. **Middle:** survival curves $t \mapsto \widehat{\mathbb{P}}(\tau_{\Delta t} > t)$. **Right:** empirical marginal of $N(T)$ conditioned on survival $\{\tau_{\Delta t} > T\}$. Parameters: $(k, m, c) = (3.0, 2.0, 0.8)$, $\rho = 0.1$, $\Delta t = 10^{-2}$, $T = 100$, $z_0 = (0.8, 0.6)$; $M = 2000$ paths per method. The estimated survivor fractions at $T = 100$ are 0.244 (event) and 0.245 (Cholesky).

The event factorization is mechanistically natural (one Brownian driver per reaction channel), whereas the Cholesky factorization is computationally economical (two-dimensional driver). Figure 11 confirms that, under the absorbed EM scheme and at the finite resolution used here, both implementations produce consistent path statistics and survival-conditioned distributions. We treat the displayed agreement as a finite-resolution diagnostic rather than as a claim of asymptotic strong or weak convergence rates for absorbed schemes.

8.4 Role of covariance: full matrix versus diagonal surrogate

The mechanistic covariance matrix Σ in (30) has a strictly negative off-diagonal entry

$$\Sigma_{12}(N, P) = -\frac{mNP}{1+N} < 0 \quad \text{for } (N, P) \in U,$$

which is the instantaneous demographic signature of the coupled predation–conversion event (Remark 5.3). To probe, at finite numerical resolution, the impact of this cross-covariance in a representative coexistence setting, we compare the full model to a diagonal surrogate with matched marginal variances,

$$\Sigma_{\text{diag}}(N, P) := \text{diag}(\Sigma_{11}(N, P), \Sigma_{22}(N, P)). \quad (53)$$

The diagonal surrogate removes instantaneous correlation ($(\Sigma_{\text{diag}})_{12} \equiv 0$) while preserving the pointwise variances.

We simulate absorbed EM paths (Section 8.2) with time step $\Delta t = 10^{-2}$ over horizon $T = 100$ using a two-dimensional Brownian driver. For the full model, we use the Cholesky factor $L_{\text{chol}}(N, P)$ satisfying $L_{\text{chol}} L_{\text{chol}}^\top = \Sigma$. For the diagonal surrogate, we use

$$L_{\text{diag}}(N, P) := \text{diag}(\sqrt{\Sigma_{11}(N, P)}, \sqrt{\Sigma_{22}(N, P)}), \quad L_{\text{diag}} L_{\text{diag}}^\top = \Sigma_{\text{diag}}.$$

Unless stated otherwise, parameters are fixed at

$$(k, m, c) = (3.0, 2.0, 0.8), \quad \rho = 0.1 \ (\Omega = 100), \quad z_0 = (0.8, 0.6),$$

and we generate $M = 2000$ independent absorbed EM trajectories for each model.

We compare two summary diagnostics:

- (i) Survival curves. Monte Carlo estimates of $t \mapsto \hat{\mathbb{P}}(\tau_{\Delta t} > t)$.
- (ii) Survival-conditioned phase-plane cloud. A snapshot of the particle cloud at $t = 100$ restricted to survivors $\{\tau_{\Delta t} > 100\}$, plotted in the (N, P) phase plane.

The goal is not to claim a universal effect of $\Sigma_{12} < 0$ across all parameters and noise levels, but rather to provide a transparent “tested-regime” diagnostic of the mechanistic correlation structure.

Figure 12 shows that, in this tested setting, the survival curves for the full model and the diagonal surrogate are close over $[0, 100]$. At the terminal time $T = 100$, the estimated survivor fractions are

$$\hat{\mathbb{P}}(\tau_{\Delta t} > 100) = 0.255 \quad (\text{full } \Sigma), \quad \hat{\mathbb{P}}(\tau_{\Delta t} > 100) = 0.247 \quad (\text{diagonal surrogate}).$$

The results show a 3.14% relative difference in survival probability at this finite Monte Carlo resolution. The survival-conditioned phase-plane clouds at $t = 100$ overlap strongly (right panel). The overlap indicates no visible factorization-level or

correlation-induced qualitative change in the distribution of surviving states at the plotted resolution.

We report this as an empirical observation in the tested regime. In other parameter regimes, for instance, closer to ∂U or at different noise amplitudes ρ , the instantaneous correlation structure may have a more pronounced impact on rare-event paths and extinction statistics.

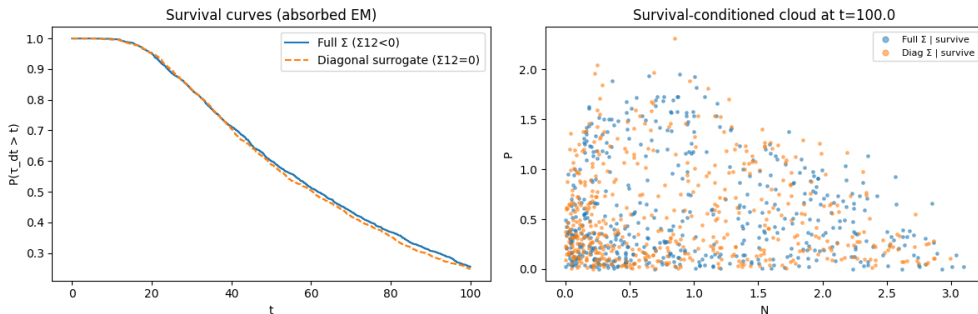


Fig. 12 Role of demographic covariance: full model vs. diagonal surrogate (tested regime). Comparative absorbed EM simulations of the mechanistic diffusion with full covariance Σ (blue, $\Sigma_{12} < 0$) and a diagonal surrogate Σ_{diag} (orange, $(\Sigma_{\text{diag}})_{12} = 0$) with matched marginal variances. **Left:** Monte Carlo survival curves $t \mapsto \hat{P}(\tau_{\Delta t} > t)$. **Right:** snapshot of the survival-conditioned particle cloud at $t = 100$ in the phase plane. Parameters: $(k, m, c) = (3.0, 2.0, 0.8)$, $\rho = 0.1$ ($\Omega = 100$), $\Delta t = 10^{-2}$, $T = 100$, $z_0 = (0.8, 0.6)$; $M = 2000$ paths per model. The estimated survivor fractions at $T = 100$ are 0.255 (full) and 0.247 (diagonal).

The comparison in Figure 12 is intended as a finite-resolution diagnostic illustrating how the mechanistic negative cross-covariance can be probed numerically. It is not a general statement that correlation is negligible. Rather, it indicates that in the tested regime above, the dominant survival statistics on the simulated horizon are not strongly sensitive to setting $\Sigma_{12} = 0$. A systematic exploration across (k, m, c, ρ) is beyond the scope of this work.

9 Discussion

This work develops a fully mechanistic stochastic Rosenzweig–MacArthur predator–prey model that respects the intrinsic irreversibility of demographic extinction. Rather than postulating an SDE with exogenous diagonal noise, we start from an event-based CTMC on \mathbb{N}_0^2 with four elementary channels (prey birth, prey competition death, predator death, and coupled predation–conversion). Absorbing coordinate axes arise naturally at the jump-process level and are preserved in the diffusion approximation by freezing trajectories upon first hitting $\partial U = \{N = 0\} \cup \{P = 0\}$. Under Kurtz density-dependent scaling, the LLN limit recovers the classical Rosenzweig–MacArthur ODE. The CLT/chemical-Langevin limit yields an Itô diffusion with explicit drift and a full instantaneous covariance matrix.

A central message is that mechanistic event coupling is not a cosmetic modeling choice. The predation–conversion increment $(-1, 1)$ necessarily induces a strictly negative cross-covariance

$$\Sigma_{12}(N, P) = -\frac{mNP}{1+N} < 0 \quad \text{on } (0, \infty)^2.$$

The negative cross-covariance is a structural “fingerprint” that cannot be reproduced by diagonal independent-noise surrogates with the same marginal variances. This feature follows directly from the reaction-channel covariance formula $\Sigma(z) = \sum_e \lambda_e(z) \Delta_e \Delta_e^\top$. The feature clarifies when independence assumptions at the SDE level become incompatible with the underlying demographic mechanism.

On the analytical side, we establish strong well-posedness up to absorption, non-explosion, and polynomial moment bounds for the full-covariance diffusion. These results ensure that the absorbed model is mathematically coherent in the ecologically relevant domain and justify interpreting boundary hits as extinction events. Qualitatively, extinction occurs with strictly positive probability from every interior initial condition for all parameter values. In the subcritical regime $m \leq c$, predator extinction occurs almost surely. The latter provides a sharp stochastic analogue of deterministic persistence thresholds. It also highlights how demographic noise, combined with boundary degeneracy, enforces eventual absorption even when interior dynamics may appear stable over finite horizons.

From a computational perspective, we record two complementary Brownian factorizations of the diffusion. The first is an event-based factorization $L_{\text{ev}} \in \mathbb{R}^{2 \times 4}$ that preserves reaction-channel structure, and the second is a two-dimensional Cholesky factorization that is often more economical in simulation. Our absorbed Euler–Maruyama implementation, together with finite-sample diagnostics, confirms practical consistency between these factorizations and offers a transparent workflow for model checking. We also compare the mechanistic diffusion to a diagonal surrogate with matched pointwise variances. The comparison illustrates how the role of Σ_{12} can be probed numerically without conflating correlation effects with variance changes. In the tested coexistence regime, survival statistics were similar across models. The similarity suggests that covariance effects may be most pronounced in other regimes rather than in typical interior fluctuations.

Several extensions follow naturally. First, systematic exploration of how $\Sigma_{12} < 0$ alters hitting-time distributions, extinction probabilities would sharpen when mechanistic covariance is essential for risk assessment. Second, developing numerical schemes with improved boundary handling (beyond clipping+freezing) and establishing convergence properties for absorbed diffusion would strengthen the computational foundation. Third, the framework readily generalizes to additional mechanistic features, including alternative functional responses, prey refuges, and multi-species networks. Among these features, event coupling may induce richer covariance structures. Finally, the model can be connected to data via likelihood-free inference. This approach would enable empirical assessment of whether mechanistic cross-covariance improves fit or predictive performance relative to diagonal-noise approximations.

In conclusion, our results provide a principled pipeline from demographic events to an absorbed full-covariance diffusion. Our model incorporates explicit drift and covariance, rigorous well-posedness up to extinction, and robust extinction statements. We expose $\Sigma_{12} < 0$ as an unavoidable mechanistic consequence of predation–conversion events. Therefore, the paper clarifies the structural limitations of ad hoc diagonal-noise SDEs and supplies a reproducible modeling and simulation blueprint for stochastic extinction analysis in consumer–resource systems.

Appendix A Non-explosion and moment bounds

This appendix proves Theorem 6.4. The argument is a standard Lyapunov–localization estimate for Itô diffusion with locally Lipschitz coefficients and at most polynomial growth. We state all steps explicitly for completeness.

Proof Set the quadratic Lyapunov function $V_q(z) := |z|^q$ for $q = 2$ or $q \geq 4$. For $R \geq 1$ define the bounded stopping time $\theta_R := \tau \wedge \sigma_R$.

A direct differentiation gives

$$\nabla V_q(z) = q|z|^{q-2}x, \quad \nabla^2 V_q(z) = q|z|^{q-2}I + q(q-2)|z|^{q-4}zz^\top.$$

Applying Itô’s formula to $V_q(Z(t \wedge \tau))$ gives

$$(\mathcal{L}V)(z) = q|z|^{q-2}\langle z, \mu(z) \rangle + \frac{q\rho^2}{2}|z|^{q-2}\text{tr}\Sigma(z) + \frac{q(q-2)\rho^2}{2}|z|^{q-4}z^\top\Sigma(z)z.$$

The positive semidefiniteness of Σ yields $z^\top\Sigma(z)z \leq |z|^2\text{tr}\Sigma(z)$. Therefore, we have

$$(\mathcal{L}V_q)(z) \leq q|z|^{q-2}\langle z, \mu(z) \rangle + \frac{q(q-1)\rho^2}{2}|z|^{q-2}\text{tr}\Sigma(z).$$

Using the explicit drift μ and covariance Σ from Section 5 (and the elementary estimate $NP \leq \frac{1}{2}(N^2 + P^2)$), one obtains a constant $C_0 < \infty$ such that for all $z \in U$,

$$\langle z, \mu(z) \rangle \leq C_0(1 + |z|^2), \quad \text{tr}\Sigma(z) \leq C_0(1 + |z|^2). \quad (\text{A1})$$

Applying (A1) and the elementary inequality $|z|^{q-2} \leq 1 + |z|^q$ gives

$$(\mathcal{L}V_q)(z) \leq C_q(1 + |z|^q) \quad (\text{A2})$$

for a constant depending on q .

By Itô’s formula applied to $V(Z(t \wedge \theta_R))$ and taking expectations, the local martingale term vanishes and we get, for $t \in [0, T]$,

$$\mathbb{E}[V(Z(t \wedge \theta_R))] = V(z_0) + \mathbb{E}\left[\int_0^{t \wedge \theta_R} (\mathcal{L}V)(Z(s)) ds\right] \leq V(z_0) + C_q \int_0^t \left(1 + \mathbb{E}[V(Z(s \wedge \theta_R))]\right) ds,$$

where we used (A2). Gronwall’s inequality yields the following bound that is uniform in R :

$$\mathbb{E}[V(Z(t \wedge \theta_R))] \leq (V(z_0) + C_q t) e^{C_q t}, \quad t \in [0, T]. \quad (\text{A3})$$

On the event $\{\sigma_R \leq T, \sigma_R < \tau\}$ one has $|Z(\theta_R)| = |Z(\sigma_R)| \geq R$ and thus $V(Z(\theta_R)) \geq R^2$. Therefore, by (A3),

$$R^2 \mathbb{P}(\sigma_R \leq T, \sigma_R < \tau) \leq \mathbb{E}[V(Z(T \wedge \theta_R))] \leq (V(z_0) + C_q T) e^{C_q T}.$$

Letting $R \rightarrow \infty$ gives $\mathbb{P}(\zeta \leq T, \zeta < \tau) = 0$. Since $T > 0$ is arbitrary, $\mathbb{P}(\zeta < \infty, \zeta < \tau) = 0$, i.e. there is no blow-up prior to boundary hitting. This proves (i).

For each $m \in \mathbb{N}_+$, consider the stopping time τ_m of Z that exits $U_m = \left(\frac{1}{m}, m\right) \times \left(\frac{1}{m}, m\right)$. Reapplying Itô's formula to $V(Z(t \wedge \tau_m))$ yields

$$\mathbb{E}[V(Z(t \wedge \tau_m))] \leq (V(z_0) + C_q t) e^{C_q t}. \quad (\text{A4})$$

Fix $q \geq 2$. Choose arbitrary $r > q$. (A4) implies that for fixed t ,

$$\sup_{m \in \mathbb{N}_+} \mathbb{E}[|Z(t \wedge \tau_m)|^r] \leq \infty.$$

Therefore, $\{|Z(t \wedge \tau_m)|^q\}_{m \in \mathbb{N}_+}$ is uniformly integrable. Since $\tau_m \rightarrow \tau$ and paths are continuous up to τ , we have $|Z(t \wedge \tau_m)|^q \rightarrow |Z(t \wedge \tau)|^q$ almost surely. Vitali's theorem yields

$$\mathbb{E}[|Z(t \wedge \tau_m)|^q] \xrightarrow{m \rightarrow \infty} \mathbb{E}[|Z(t \wedge \tau)|^q].$$

Taking limit in $m \rightarrow \infty$ in (A4) gives

$$\mathbb{E}[V(Z(t \wedge \tau))] \leq (V(z_0) + C_q t) e^{C_q t}. \quad (\text{A5})$$

Taking supremum in $t \in [0, T]$ in (A5) gives

$$\sup_{0 \leq t \leq T} \mathbb{E}[V(Z(t \wedge \tau))] \leq C_{p,T}(1 + V(z_0)) = C_{p,T}(1 + |z_0|^q)$$

for some $C_{p,T} > 0$. \square

Appendix B Proof of Theorem 7.4

In this appendix we give a complete proof of Theorem 7.4: for every $z \in U = (0, \infty)^2$,

$$\mathbb{P}_z(\tau < \infty) > 0, \quad \tau := \inf\{t > 0 : N(t) = 0 \text{ or } P(t) = 0\}.$$

B.1 Positive density on a compact set away from the boundary

We work with the interior strong solution $Z(t) = (N(t), P(t))$ of

$$dZ(t) = \mu(Z(t)) dt + \rho L_{\text{ev}}(Z(t)) dW(t), \quad Z(0) = z \in U, \quad (\text{B6})$$

where μ and $\Sigma = L_{\text{ev}} L_{\text{ev}}^\top$ are given by (29)–(30). Recall in particular

$$\mu_2(N, P) = \left(\frac{mN}{1+N} - c\right)P, \quad \Sigma_{22}(N, P) = \left(c + \frac{mN}{1+N}\right)P, \quad (N, P) \in U. \quad (\text{B7})$$

Fix $z = (N_0, P_0) \in U$ and define

$$a := \frac{1}{2} \min\{N_0, P_0, 1\}, \quad b := 2 \max\{N_0, P_0, 1\}. \quad (\text{B8})$$

For $0 < a < b$ and $\varepsilon > 0$ define

$$K_{a,b} := [a, b] \times [a, b] \Subset U, \quad G_{a,b,\varepsilon} := [a, b] \times (0, \varepsilon) \subset U.$$

Then $0 < a < b < \infty$ and $z \in K_{a,b}$.

Lemma B.1 (Staying inside $K_{a,b}$ for a short time) *There exists $t_0 = t_0(z) > 0$ such that*

$$\mathbb{P}_z(Z(t) \in K_{a,b} \text{ for all } t \in [0, t_0]) > 0.$$

Proof Since $z \in \text{int}(K_{a,b})$ and sample paths are continuous, the exit time $\eta := \inf\{t \geq 0 : Z(t) \notin K_{a,b}\}$ satisfies $\mathbb{P}_z(\eta > 0) = 1$. Hence $\mathbb{P}_z(\eta > t_0) > 0$ for some $t_0 > 0$. \square

On $K_{a,b}$ the diffusion matrix is uniformly elliptic and smooth.

Lemma B.2 (Uniform ellipticity on $K_{a,b}$) *There exists $\lambda_{a,b} > 0$ such that for all $(N, P) \in K_{a,b}$ and all $\xi \in \mathbb{R}^2$,*

$$\xi^\top \Sigma(N, P) \xi \geq \lambda_{a,b} |\xi|^2.$$

Proof By Lemma 5.2, Σ is positive definite on U . By continuity of Σ and compactness of $K_{a,b} \Subset U$, the smallest eigenvalue of Σ attains a strictly positive minimum on $K_{a,b}$. \square

We use a standard heat-kernel lower bound on compacts. We state it at the level we need.

Lemma B.3 (Small-ball lower bound for the killed transition kernel) *Fix $t > 0$. For each $x \in U$, the killed kernel*

$$P_t(x, dy) := \mathbb{P}_x(Z(t) \in dy, t < \tau)$$

is absolutely continuous with respect to Lebesgue measure on U ; we denote its Radon–Nikodym density by $p_t(x, \cdot)$, i.e.

$$P_t(x, A) = \int_A p_t(x, y) dy, \quad A \subset U \text{ Borel.}$$

Moreover, for each compact $K \Subset U$ there exist constants $c_K(t) > 0$ and $r_K(t) > 0$ such that

$$P_t(x, B(y, r)) \geq c_K(t) |B(y, r)|, \quad \forall x, y \in K, \forall r \in (0, r_K(t)]. \quad (\text{B9})$$

Proof We show absolute continuity of $P_t(x, \cdot)$. Fix $x \in U$ and $t > 0$. For $R \geq 1$ define the bounded domain

$$D_R := U \cap B(0, R), \quad \tau_R := \inf\{s \geq 0 : Z(s) \notin D_R\}.$$

Consider the killed-in- D_R kernel

$$P_t^{(R)}(x, A) := \mathbb{P}_x(Z(t) \in A, t < \tau_R), \quad A \subset D_R \text{ Borel.}$$

D_R is bounded and the coefficients are smooth and uniformly elliptic on $\overline{D_R}$ away from the axes. Therefore, by standard parabolic theory for uniformly elliptic operators with Dirichlet boundary, $P_t^{(R)}(x, \cdot)$ admits a (Dirichlet) transition density $p_t^{(R)}(x, \cdot)$ with respect to Lebesgue measure on D_R :

$$P_t^{(R)}(x, A) = \int_A p_t^{(R)}(x, y) dy, \quad A \subset D_R.$$

In particular, $P_t^{(R)}(x, \cdot) \ll dy$.

Moreover, for any Borel set $A \subset U$,

$$P_t^{(R)}(x, A) = \mathbb{P}_x(Z(t) \in A, t < \tau_R) \uparrow \mathbb{P}_x(Z(t) \in A, t < \tau) =: P_t(x, A), \quad R \rightarrow \infty,$$

since $\tau_R \uparrow \tau$ almost surely (continuity of paths and $D_R \uparrow U$). Therefore, if A is Lebesgue-null, then for every R , $P_t^{(R)}(x, A) = 0$, hence $P_t(x, A) = \lim_{R \rightarrow \infty} P_t^{(R)}(x, A) = 0$. This shows $P_t(x, \cdot) \ll dy$. By the Radon–Nikodym theorem there exists a density $p_t(x, \cdot)$ such that

$$P_t(x, A) = \int_A p_t(x, y) dy, \quad A \subset U.$$

We establish the small-ball lower bound on a compact $K \Subset U$. Fix a compact set $K \Subset U$. Choose a bounded C^2 domain D such that

$$K \Subset D \Subset U, \quad \text{dist}(D, \partial U) > 0.$$

Let $\tau_D := \inf\{s \geq 0 : Z(s) \notin D\}$ and define the killed-in- D kernel

$$P_t^D(x, A) := \mathbb{P}_x(Z(t) \in A, t < \tau_D), \quad A \subset D.$$

Since $D \Subset U$, one has $\{t < \tau_D\} \subset \{t < \tau\}$ and therefore

$$P_t(x, A) \geq P_t^D(x, A), \quad x \in U, A \subset D. \quad (\text{B10})$$

On \overline{D} the diffusion matrix is uniformly elliptic and the coefficients are smooth. Hence, the killed kernel P_t^D admits a Dirichlet heat-kernel density $p_t^D(x, y)$ on $D \times D$ which is continuous and strictly positive for each fixed $t > 0$. In particular, the continuous function $(x, y) \mapsto p_t^D(x, y)$ attains a strictly positive minimum on the compact set $K \times K$:

$$m_K(t) := \inf_{x \in K} \inf_{y \in K} p_t^D(x, y) > 0.$$

Let

$$r_K(t) := \frac{1}{2} \text{dist}(K, \partial D) > 0.$$

Then for every $y \in K$ and $r \in (0, r_K(t)]$ we have $B(y, r) \subset D$. Therefore, for $x, y \in K$ and $r \in (0, r_K(t)]$, using (B10) and integrating the heat kernel,

$$P_t(x, B(y, r)) \geq P_t^D(x, B(y, r)) = \int_{B(y, r)} p_t^D(x, z) dz \geq \int_{B(y, r)} m_K(t) dz = m_K(t) |B(y, r)|.$$

Thus (B9) holds with $c_K(t) := m_K(t)$. \square

Choose a point $y_* = (N_*, P_*)$ with $N_* = a$ and $P_* = \varepsilon_*/2$. Take $r > 0$ small so that

$$B(y_*, r) \subset [a/2, 2a] \times (0, \varepsilon_*).$$

Pick a compact $K' \Subset U$ such that

$$K_{a,b} \cup \overline{B(y_*, r)} \subset K'.$$

Lemma B.3 yields the following bound:

$$\inf_{x \in K_{a,b}} \mathbb{P}_x(Z(t_2) \in B(y_*, r), t_2 < \tau) \geq c_{K'}(t_2) |B(y_*, r)| > 0.$$

Using the strong Markov property at time t_1 ,

$$\mathbb{P}_z(Z(t_1 + t_2) \in B(y_*, r), t_1 + t_2 < \tau) \geq \mathbb{P}_z(t_1 < \tau, Z(t_1) \in K_{a,b}) \cdot c > 0.$$

Since $B(y_*, r) \subset [a/2, 2a] \times (0, \varepsilon_*)$ we conclude

$$\mathbb{P}_z(Z(t_1 + t_2) \in [a/2, 2a] \times (0, \varepsilon_*), t_1 + t_2 < \tau) > 0. \quad (\text{B11})$$

Define the thin set

$$G := G_{a/2, 2a, \varepsilon_*} = [a/2, 2a] \times (0, \varepsilon_*).$$

Equation (B11) says: starting from z , the process enters G at time $T := t_1 + t_2$ with positive probability while still alive.

B.2 One-dimensional comparison inside G

Fix the thin set $G = [a/2, 2a] \times (0, \varepsilon_*)$ and define the exit time

$$\sigma := \inf\{t \geq 0 : Z(t) \notin [a/4, 4a] \times (0, 2\varepsilon_*)\}.$$

On $[0, \sigma)$ we have $N(t) \in [a/4, 4a]$ and $P(t) \in (0, 2\varepsilon_*)$.

On this region we bound the predator drift and diffusion uniformly.

Lemma B.4 (Uniform bounds on the predator coefficients on the strip) *There exist constants $\kappa \in \mathbb{R}$ and $\alpha > 0$, depending only on (a, m, c) , such that for all $(N, P) \in [a/4, 4a] \times (0, 2\varepsilon_*)$,*

$$\mu_2(N, P) \leq \kappa P, \quad (\text{B12})$$

and

$$\Sigma_{22}(N, P) \geq \alpha P. \quad (\text{B13})$$

Proof Since $N \mapsto \frac{mN}{1+N}$ is increasing,

$$\frac{mN}{1+N} - c \leq \frac{m(4a)}{1+4a} - c =: \kappa,$$

which gives (B12). Also,

$$c + \frac{mN}{1+N} \geq c + \frac{m(a/4)}{1+a/4} =: \alpha > 0,$$

and using (B7) gives (B13). \square

We compare to a one-dimensional square-root diffusion. Consider the process

$$dY(t) = \kappa Y(t) dt + \rho \sqrt{\alpha Y(t)} dB(t), \quad Y(0) = p \in (0, \varepsilon_*), \quad (\text{B14})$$

where B is a standard one-dimensional Brownian motion.

Lemma B.5 (CIR hits 0 before leaving $(0, 2\varepsilon_*)$ with positive probability) *Let Y solve*

$$dY(t) = \kappa Y(t) dt + \rho \sqrt{\alpha Y(t)} dB(t), \quad Y(0) = p \in (0, \varepsilon_*),$$

with constants $\rho > 0$, $\alpha > 0$, and $\kappa \in \mathbb{R}$. Set

$$\tau_0 := \inf\{t \geq 0 : Y(t) = 0\}, \quad \tau_{2\varepsilon_*} := \inf\{t \geq 0 : Y(t) \geq 2\varepsilon_*\}.$$

Then

$$\mathbb{P}_p(\tau_0 < \tau_{2\varepsilon_*}) > 0.$$

Proof By the scaling $X(t) := \frac{4}{\rho^2 \alpha} Y(t)$, the process X satisfies

$$dX(t) = \kappa X(t) dt + 2\sqrt{X(t)} dB(t),$$

i.e. X is a square-root diffusion of CIR/BESQ(0) type (zero mean-reversion level). In particular, the boundary 0 is accessible and is hit in finite time almost surely: for every $x > 0$,

$$\mathbb{P}_x(\inf\{t \geq 0 : X(t) = 0\} < \infty) = 1,$$

see (Revuz and Yor 1999). Returning to Y yields $\mathbb{P}_p(\tau_0 < \infty) = 1$ for all $p > 0$.

Now fix $\tilde{b} := 2\varepsilon_*$ and define

$$u(p) := \mathbb{P}_p(\tau_0 < \tau_{\tilde{b}}), \quad p \in (0, \tilde{b}).$$

By continuity of paths, $\tau_0 \wedge \tau_{\tilde{b}} > 0$ a.s. and $Y(\tau_0 \wedge \tau_{\tilde{b}}) \in \{0, \tilde{b}\}$ a.s. Moreover, by the strong Markov property, u is the unique bounded solution of the Dirichlet boundary value problem

$$\mathcal{L}u = 0 \text{ on } (0, \tilde{b}), \quad u(0) = 1, \quad u(\tilde{b}) = 0,$$

where $\mathcal{L}f(y) = \kappa y f'(y) + \frac{\rho^2 \alpha}{2} y f''(y)$ is the generator of Y on $(0, \infty)$. Since u is continuous on $[0, \tilde{b}]$ with distinct boundary values and satisfies the maximum principle for one-dimensional diffusions, it follows that $0 < u(p) < 1$ for all $p \in (0, \tilde{b})$. In particular, for $p \in (0, \varepsilon_*) \subset (0, \tilde{b})$ we have $u(p) > 0$, i.e. $\mathbb{P}_p(\tau_0 < \tau_{2\varepsilon_*}) > 0$. \square

Lemma B.6 (Strip-hitting bound) *Fix $b > 0$ and $x = (n, p) \in [a/2, 2a] \times (0, b/2)$. Let*

$$\tau_0^P := \inf\{t \geq 0 : P(t) = 0\}, \quad \tau_b^P := \inf\{t \geq 0 : P(t) \geq b\}, \quad \sigma_N := \inf\{t \geq 0 : N(t) \notin [a/4, 4a]\},$$

and $\theta := \tau_0^P \wedge \tau_b^P \wedge \sigma_N$. Assume that on $\{t < \sigma_N\}$,

$$\mu_2(N(t), P(t)) \leq \kappa P(t), \quad \Sigma_{22}(N(t), P(t)) \geq \alpha P(t),$$

for constants $\kappa \in \mathbb{R}$ and $\alpha > 0$. Let Y be the CIR diffusion

$$dY(t) = \kappa_+ Y(t) dt + \rho \sqrt{\alpha Y(t)} dB(t), \quad \kappa_+ := \max\{\kappa, 0\},$$

and define $u(r) := \mathbb{P}_r(\tau_0^Y < \tau_b^Y)$. Then for every such $x = (n, p)$,

$$\mathbb{P}_x(\tau_0^P < \tau_b^P \wedge \sigma_N) \geq u(p) - \mathbb{P}_x(\sigma_N < \tau_0^P \wedge \tau_b^P).$$

Proof Let $v(r) := \mathbb{P}_r(\tau_b^Y < \tau_0^Y) = 1 - u(r)$. Then $v \in C^2((0, b)) \cap C([0, b])$ solves

$$\kappa_+ r v'(r) + \frac{\rho^2 \alpha}{2} r v''(r) = 0, \quad v(0) = 0, \quad v(b) = 1,$$

and satisfies $v' \geq 0$.

Set $\theta = \tau_0^P \wedge \tau_b^P \wedge \sigma_N$. Applying Itô to $v(P(t \wedge \theta))$ and using $\mu_2 \leq \kappa P \leq \kappa_+ P$ together with $\Sigma_{22} \geq \alpha P$ and $v' \geq 0$ yields that $v(P(t \wedge \theta))$ is a bounded supermartingale. Hence

$$v(p) \geq \mathbb{E}_x[v(P(\theta))].$$

Now decompose into the disjoint events

$$\text{I} = \{\tau_0^P < \tau_b^P \wedge \sigma_N\}, \quad \text{II} = \{\tau_b^P < \tau_0^P \wedge \sigma_N\}, \quad \text{III} = \{\sigma_N < \tau_0^P \wedge \tau_b^P\}.$$

On II we have $P(\theta) = b$ hence $v(P(\theta)) = 1$. On I we have $P(\theta) = 0$ hence $v(P(\theta)) = 0$. On III we only know $0 \leq v(P(\theta)) \leq 1$. Therefore

$$\mathbb{E}_x[v(P(\theta))] = \mathbb{P}_x(\text{II}) + \mathbb{E}_x[v(P(\theta)) ; \text{III}] \geq \mathbb{P}_x(\text{II}).$$

Thus $\mathbb{P}_x(\text{II}) \leq v(p)$ and consequently

$$\mathbb{P}_x(\text{I}) = 1 - \mathbb{P}_x(\text{II}) - \mathbb{P}_x(\text{III}) \geq 1 - v(p) - \mathbb{P}_x(\text{III}) = u(p) - \mathbb{P}_x(\sigma_N < \tau_0^P \wedge \tau_b^P),$$

which is the claim. \square

Lemma B.7 (Uniform strip-hitting probability on G) Fix $a > 0$ and $\varepsilon_* > 0$, and set

$$G := [a/2, 2a] \times (0, \varepsilon_*), \quad b := 2\varepsilon_*.$$

Let $\tau_0^P, \tau_b^P, \sigma_N$ be as in Lemma B.6. Assume that there exist constants $\kappa \in \mathbb{R}$ and $\alpha > 0$ such that on $\{t < \sigma_N\}$,

$$\mu_2(N(t), P(t)) \leq \kappa P(t), \quad \Sigma_{22}(N(t), P(t)) \geq \alpha P(t).$$

Then there exists $q_* > 0$ such that

$$\inf_{x \in G} \mathbb{P}_x(\tau_0^P < \tau_b^P \wedge \sigma_N) \geq q_*. \quad (\text{B15})$$

One convenient choice is

$$q_* := \frac{1}{2} u(\varepsilon_*), \quad u(r) := \mathbb{P}_r(\tau_0^Y < \tau_b^Y),$$

provided $\varepsilon_* > 0$ is chosen so that

$$\sup_{x \in G} \mathbb{P}_x(\sigma_N < \tau_0^P \wedge \tau_b^P) \leq \frac{1}{2} u(\varepsilon_*). \quad (\text{B16})$$

Proof Fix $x = (n, p) \in G$. Apply Lemma B.6 with $b = 2\varepsilon_*$ to obtain

$$\mathbb{P}_x(\tau_0^P < \tau_b^P \wedge \sigma_N) \geq u(p) - \mathbb{P}_x(\sigma_N < \tau_0^P \wedge \tau_b^P).$$

Since $p \in (0, \varepsilon_*)$ and $u(\cdot)$ is decreasing in the initial condition (starting closer to 0 can only increase the chance of hitting 0 before b), we have $u(p) \geq u(\varepsilon_*)$. Hence

$$\mathbb{P}_x(\tau_0^P < \tau_b^P \wedge \sigma_N) \geq u(\varepsilon_*) - \mathbb{P}_x(\sigma_N < \tau_0^P \wedge \tau_b^P).$$

If (B16) holds, then the right-hand side is bounded below by $\frac{1}{2}u(\varepsilon_*)$, uniformly in $x \in G$. Taking the infimum over $x \in G$ yields (B15). \square

Proof of Theorem 7.4 Let $z \in U$ be arbitrary. By (B11), there exists $T > 0$ such that

$$\mathbb{P}_z(Z(T) \in G, T < \tau) > 0.$$

Let $b = 2\varepsilon_*$ and σ_N be the prey-exit time from $[a/4, 4a]$ as above, and define the stopping time

$$\sigma := \tau_0^P \wedge \tau_b^P \wedge \sigma_N.$$

On the event $\{\tau_0^P = \sigma\}$ the process hits the boundary $\{P = 0\} \subset \partial U$ and hence $\tau < \infty$ under the absorbed convention. Therefore,

$$\mathbb{P}_x(\tau < \infty) \geq \mathbb{P}_x(\tau_0^P < \tau_b^P \wedge \sigma_N), \quad x \in G.$$

By Lemma B.7, there exists $q_* > 0$ such that

$$\inf_{x \in G} \mathbb{P}_x(\tau < \infty) \geq q_*.$$

Apply the strong Markov property at time T :

$$\begin{aligned} \mathbb{P}_z(\tau < \infty) &\geq \mathbb{E}_z \left[\mathbf{1}_{\{Z(T) \in G, T < \tau\}} \mathbb{P}_{Z(T)}(\tau < \infty) \right] \\ &\geq q_* \mathbb{P}_z(Z(T) \in G, T < \tau) > 0. \end{aligned}$$

This proves $\mathbb{P}_z(\tau < \infty) > 0$ for all $z \in U$. \square

Appendix C A hitting lemma for subcritical extinction

This appendix supplies the one-dimensional boundary-hitting input used in Theorem 7.5. We record a domination statement matching the usage in Theorem 7.5.

Lemma C.1 (A convenient domination form) *Let P be a nonnegative continuous semi-martingale on $[0, \tau)$ of the form*

$$dP_t = a_t P_t dt + dM_t, \quad P_0 > 0,$$

where $a_t \leq 0$ for all $t < \tau$ and M is a continuous local martingale satisfying

$$d\langle M \rangle_t \geq \rho^2 c P_t dt \quad \text{for all } t < \tau,$$

for some constants $\rho > 0$ and $c > 0$. Then

$$\tau_0 := \inf\{t \geq 0 : P_t = 0\} < \infty \quad \text{almost surely.}$$

Proof We remove the drift by an exponential transform. Define the adapted finite-variation process

$$A_t := \int_0^t a_s ds \leq 0, \quad t < \tau,$$

and set

$$X_t := e^{-A_t} P_t, \quad t < \tau.$$

Since A has finite variation, Itô's formula for products yields, on $[0, \tau)$,

$$dX_t = e^{-A_t} dP_t + P_t d(e^{-A_t}) = e^{-A_t} (a_t P_t dt + dM_t) - e^{-A_t} a_t P_t dt = e^{-A_t} dM_t.$$

Hence X is a continuous local martingale on $[0, \tau)$. Moreover, $X_t \geq 0$ for all $t < \tau$ because $P_t \geq 0$ and $e^{-A_t} > 0$. Finally, $X_t = 0$ iff $P_t = 0$ (since $e^{-A_t} > 0$), so the hitting times of 0 coincide:

$$\tau_0 = \inf\{t \geq 0 : P_t = 0\} = \inf\{t \geq 0 : X_t = 0\}.$$

Thus it suffices to show that X hits 0 in finite time a.s.

We establish a square-root-type lower bound for the quadratic variation of X . Since $X_t = \int_0^t e^{-A_s} dM_s + X_0$, we have

$$d\langle X \rangle_t = e^{-2A_t} d\langle M \rangle_t.$$

Using the assumed bound $d\langle M \rangle_t \geq \rho^2 c P_t dt$ and $P_t = e^{A_t} X_t$, we obtain

$$d\langle X \rangle_t \geq e^{-2A_t} \rho^2 c P_t dt = \rho^2 c e^{-A_t} X_t dt \geq \rho^2 c X_t dt, \quad t < \tau, \quad (\text{C17})$$

where we used $e^{-A_t} \geq 1$ because $A_t \leq 0$.

Let

$$Q_t := \langle X \rangle_{t \wedge \tau_0}, \quad t \geq 0.$$

Then Q_t is continuous and nondecreasing. By the Dambis–Dubins–Schwarz theorem applied to the continuous local martingale $X_{t \wedge \tau_0}$, there exists a standard one-dimensional Brownian motion B such that

$$X_{t \wedge \tau_0} = X_0 + B_{Q_t}, \quad t \geq 0. \quad (\text{C18})$$

Assume for contradiction that $\mathbb{P}(\tau_0 = \infty) > 0$ and work on the event $\{\tau_0 = \infty\}$. Then $X_t > 0$ for all $t \geq 0$ and (C18) holds for all $t \geq 0$ with $Q_t = \langle X \rangle_t$.

We claim that on $\{\tau_0 = \infty\}$ one must have $\langle X \rangle_\infty = \infty$. Indeed, if $\langle X \rangle_\infty < \infty$, then Q_t converges to a finite limit Q_∞ and hence X_t converges almost surely to

$$X_\infty = X_0 + B_{Q_\infty}.$$

Since B_{Q_∞} has a continuous distribution conditional on Q_∞ , we have $\mathbb{P}(X_\infty = 0, Q_\infty < \infty) = 0$. Thus on $\{\tau_0 = \infty, Q_\infty < \infty\}$ we have $X_\infty > 0$ almost surely. But then $\int_0^\infty X_s ds = \infty$ on that event (because $X_s \rightarrow X_\infty > 0$), and integrating (C17) yields

$$\langle X \rangle_\infty \geq \rho^2 c \int_0^\infty X_s ds = \infty,$$

a contradiction. Hence, on $\{\tau_0 = \infty\}$ we must have $\langle X \rangle_\infty = \infty$.

Now let

$$\sigma := \inf\{u \geq 0 : B_u = -X_0\}.$$

For Brownian motion, $\sigma < \infty$ almost surely. Since $Q_t = \langle X \rangle_t$ is continuous, nondecreasing, and diverges to ∞ on $\{\tau_0 = \infty\}$, there exists a (random) time t_σ such that $Q_{t_\sigma} = \sigma$. Evaluating (C18) at t_σ gives

$$X_{t_\sigma} = X_0 + B_\sigma = 0,$$

contradicting $\tau_0 = \infty$. Therefore $\mathbb{P}(\tau_0 = \infty) = 0$, i.e. $\tau_0 < \infty$ almost surely.

Since $P_t = e^{A_t} X_t$ with $e^{A_t} > 0$, P hits 0 at the same time as X . Hence $\inf\{t \geq 0 : P_t = 0\} < \infty$ almost surely, completing the proof. \square

Data Availability:

Data sharing is not applicable to this article, as no new data was created or analyzed in this study. All simulations are reproducible; code and scripts are provided on demand.

Author Contribution:

All authors have accepted responsibility for the entire content of this manuscript and approved its submission.

Declaration:

All authors declare no competing interests.

References

Abundo, M.: A stochastic model for predator-prey systems: basic properties, stability and computer simulation. *Journal of Mathematical Biology* **29**(6), 495–511 (1991) <https://doi.org/10.1007/BF00164048>

Anderson, D.F., Higham, D.J., Leite, S.C., Williams, R.J.: On constrained langevin equations and (bio)chemical reaction networks. *Multiscale Modeling & Simulation* **17**(1), 1–30 (2019) <https://doi.org/10.1137/18M1190999>

Anderson, D.F., Kurtz, T.G.: Continuous time markov chain models for chemical reaction networks. In: *Design and Analysis of Biomolecular Circuits*, pp. 3–42. Springer, New York, NY (2011). https://doi.org/10.1007/978-1-4419-6766-4_1

Allen, L.J.S.: Stochastic Population and Epidemic Models: Persistence and Extinction. Springer, Cham (2015). <https://doi.org/10.1007/978-3-319-21554-9>

Barraquand, F., Louca, S., Abbott, K.C., Cobbold, C.A., Cordoleani, F., DeAngelis, D.L.: Moving forward in circles: challenges and opportunities in modelling population cycles. *Ecology Letters* **20**(8), 1074–1092 (2017) <https://doi.org/10.1111/ele.12789>

Cheng, K.-S.: Uniqueness of a limit cycle for a predator-prey system. *SIAM Journal on Mathematical Analysis* **12**(4), 541–548 (1981) <https://doi.org/10.1137/0512047>

Ethier, S.N., Kurtz, T.G.: Markov Processes: Characterization and Convergence, 1st edn. Wiley Series in Probability and Statistics. Wiley, New York (1986). <https://doi.org/10.1002/9780470316658>

Gibson, M.A., Bruck, J.: Efficient exact stochastic simulation of chemical systems with many species and many channels. *The Journal of Physical Chemistry A* **104**(9), 1876–1889 (2000) <https://doi.org/10.1021/jp993732q>

Grunert, K., Holden, H., Jakobsen, E.R., Stenseth, N.C.: Evolutionarily stable strategies in stable and periodically fluctuating populations: The Rosenzweig–MacArthur predator–prey model. *Proceedings of the National Academy of Sciences* **118**(4), 2017463118 (2021) <https://doi.org/10.1073/pnas.2017463118>

Gillespie, D.T.: A general method for numerically simulating the stochastic time evolution of coupled chemical reactions. *Journal of Computational Physics* **22**(4), 403–434 (1976) [https://doi.org/10.1016/0021-9991\(76\)90041-3](https://doi.org/10.1016/0021-9991(76)90041-3)

Gillespie, D.T.: Exact stochastic simulation of coupled chemical reactions. *The Journal of Physical Chemistry* **81**(25), 2340–2361 (1977) <https://doi.org/10.1021/j100540a008>

Gillespie, D.T.: The chemical Langevin equation. *The Journal of Chemical Physics* **113**(1), 297–306 (2000) <https://doi.org/10.1063/1.481811>

Gillespie, D.T.: The chemical Langevin and fokker-planck equations for the reversible isomerization reaction. *The Journal of Physical Chemistry A* **106**(20), 5063–5071 (2002) <https://doi.org/10.1021/jp0128832>

Gounand, I., Mouquet, N., Canard, E., Guichard, F., Hauzy, C., Gravel, D.: The paradox of enrichment in metaecosystems. *The American Naturalist* **184**(6), 752–763 (2014) <https://doi.org/10.1086/678406>

Holling, C.S.: Some characteristics of simple types of predation and parasitism. *The Canadian Entomologist* **91**(7), 385–398 (1959) <https://doi.org/10.4039/Ent91385-7>

Hobolth, A., Stone, E.A.: Simulation from endpoint-conditioned, continuous-time

Markov chains on a finite state space, with applications to molecular evolution. The Annals of Applied Statistics **3**(3) (2009) <https://doi.org/10.1214/09-AOAS247>

Huang, Y., Shi, W., Wei, C., Zhang, S.: A stochastic predator–prey model with Holling II increasing function in the predator. Journal of Biological Dynamics **15**(1), 1–18 (2021) <https://doi.org/10.1080/17513758.2020.1859146>

Ikeda, N., Watanabe, S.: Stochastic Differential Equations and Diffusion Processes. North-Holland mathematical library, vol. v. 24. North-Holland Pub. Co. Kodansha Sole distributors for the U.S.A. and Canada, Elsevier North-Holland, Amsterdam New York Tokyo New York, NY (1981)

Jeanblanc, M., Yor, M., Chesney, M.: Mathematical Methods for Financial Markets. Springer, London (2009). <https://doi.org/10.1007/978-1-84628-737-4>

Jiang, X., Zu, L., Jiang, D., O'Regan, D.: Analysis of a stochastic holling type II predator–prey model under regime switching. Bulletin of the Malaysian Mathematical Sciences Society **43**(3), 2171–2197 (2020) <https://doi.org/10.1007/s40840-019-00798-6>

Kampen, N.G.V.: A power series expansion of the master equation. Canadian Journal of Physics **39**(4), 551–567 (1961) <https://doi.org/10.1139/p61-056>

Kampen, N.G.v.: Stochastic Processes in Physics and Chemistry, 3rd ed edn. North-Holland personal library. Elsevier, Amsterdam, The Netherlands Oxford, UK (2007). <https://doi.org/10.1016/B978-0-444-52965-7.X5000-4>

Korner-Nievergelt, F., Roth, T., Von Felten, S., Guélat, J., Almasi, B., Korner-Nievergelt, P.: Markov chain monte carlo simulation. In: Bayesian Data Analysis in Ecology Using Linear Models with R, BUGS, and STAN, pp. 197–212. Elsevier, Boston (2015). <https://doi.org/10.1016/B978-0-12-801370-0.00012-5>

Karatzas, I., Shreve, S.E.: Brownian Motion and Stochastic Calculus. Graduate Texts in Mathematics, vol. 113. Springer, New York, NY (1998). <https://doi.org/10.1007/978-1-4612-0949-2>

Kurtz, T.G.: Solutions of ordinary differential equations as limits of pure jump markov processes. Journal of Applied Probability **7**(1), 49–58 (1970) <https://doi.org/10.2307/3212147>

Kurtz, T.G.: Limit theorems for sequences of jump Markov processes approximating ordinary differential processes. Journal of Applied Probability **8**(2), 344–356 (1971) <https://doi.org/10.2307/3211904>

Kurtz, T.G.: Limit theorems and diffusion approximations for density dependent Markov chains. In: Stochastic Systems: Modeling, Identification and Optimization, I vol. 5, pp. 67–78. Springer, Berlin, Heidelberg (1976). <https://doi.org/10.1007/BFb0120765>. Series Title: Mathematical Programming Studies

Kurtz, T.G.: Strong approximation theorems for density dependent Markov chains. *Stochastic Processes and their Applications* **6**(3), 223–240 (1978) [https://doi.org/10.1016/0304-4149\(78\)90020-0](https://doi.org/10.1016/0304-4149(78)90020-0)

Lande, R., Engen, S., Saether, B.-E.: *Stochastic Population Dynamics in Ecology and Conservation*. Oxford University Press, Oxford (2003). <https://doi.org/10.1093/acprof:oso/9780198525257.001.0001>

Leite, S.C., Williams, R.J.: A constrained Langevin approximation for chemical reaction networks. *The Annals of Applied Probability* **29**(3) (2019) <https://doi.org/10.1214/18-AAP1421>

Liu, Z., Wang, L.S., Yu, J., Zhang, J., Martel, E., Li, S.: Bidirectional endothelial feedback drives turing-vascular patterning and drug-resistance niches: a hybrid PDE-agent-based study. *Bioengineering* **12**(10), 1097 (2025) <https://doi.org/10.3390/bioengineering12101097>

Liang, Y., Wang, L.S., Yu, J., Liu, Z.: Global well-posedness and stability of nonlocal damage-structured lineage model with feedback and dedifferentiation. *Mathematics* **13**(22), 3583 (2025) <https://doi.org/10.3390/math13223583>

Manninen, T., Linne, M.-L., Ruohonen, K.: Developing Itô stochastic differential equation models for neuronal signal transduction pathways. *Computational Biology and Chemistry* **30**(4), 280–291 (2006) <https://doi.org/10.1016/j.compbiochem.2006.04.002>

Murray, J.D. (ed.): *Mathematical Biology: I. An Introduction. Interdisciplinary Applied Mathematics*, vol. 17. Springer, New York, NY (2002). <https://doi.org/10.1007/b98868>

Nåsell, I.: Extinction and quasi-stationarity in the verhulst logistic model. *Journal of Theoretical Biology* **211**(1), 11–27 (2001) <https://doi.org/10.1006/jtbi.2001.2328>

Øksendal, B.: *Stochastic Differential Equations*. Universitext. Springer, Berlin, Heidelberg (2003). <https://doi.org/10.1007/978-3-642-14394-6>

Ovaskainen, O., Meerson, B.: Stochastic models of population extinction. *Trends in Ecology & Evolution* **25**(11), 643–652 (2010) <https://doi.org/10.1016/j.tree.2010.07.009>

Rosenzweig, M.L., MacArthur, R.H.: Graphical representation and stability conditions of predator-prey interactions. *The American Naturalist* **97**(895), 209–223 (1963). Accessed 2026-02-01

Rosenzweig, M.L.: Paradox of enrichment: destabilization of exploitation ecosystems in ecological time. *Science* **171**(3969), 385–387 (1971) <https://doi.org/10.1126/science.171.3969.385>

Revuz, D., Yor, M.: Continuous Martingales and Brownian Motion. Grundlehren der mathematischen Wissenschaften, vol. 293. Springer, Berlin, Heidelberg (1999). <https://doi.org/10.1007/978-3-662-06400-9>

Szpruch, L., Higham, D.J.: Comparing hitting time behavior of markov jump processes and their diffusion approximations. *Multiscale Modeling & Simulation* **8**(2), 605–621 (2010) <https://doi.org/10.1137/090750202>

Sugie, J., Saito, Y.: Uniqueness of limit cycles in a rosenzweig–MacArthur model with prey immigration. *SIAM Journal on Applied Mathematics* **72**(1), 299–316 (2012) <https://doi.org/10.1137/11084008X>

Wallace, E.W.J., Gillespie, D.T., Sanft, K.R., Petzold, L.R.: Linear noise approximation is valid over limited times for any chemical system that is sufficiently large. *IET Systems Biology* **6**(4), 102–115 (2012) <https://doi.org/10.1049/iet-syb.2011.0038>

Wilkie, J., Wong, Y.M.: Positivity preserving chemical Langevin equations. *Chemical Physics* **353**(1-3), 132–138 (2008) <https://doi.org/10.1016/j.chemphys.2008.08.001>

Wang, L.S., Yu, J.: Analysis framework for stochastic predator–prey model with demographic noise. *Results in Applied Mathematics* **27**, 100621 (2025) <https://doi.org/10.1016/j.rinam.2025.100621>

Wang, L.S., Yu, J.: Algebraic–spectral thresholds and discrete–continuous stability transfer in leslie–gower systems. *Electronic Research Archive* **34**(1), 251–290 (2026) <https://doi.org/10.3934/era.2026013>

Wang, L.S., Yu, J., Li, S., Liu, Z.: Analysis and mean-field limit of a hybrid PDE-ABM modeling angiogenesis-regulated resistance evolution. *Mathematics* **13**(17), 2898 (2025) <https://doi.org/10.3390/math13172898>

Zhang, X.: The global dynamics of stochastic Holling type II predator-prey models with non constant mortality rate. *Filomat* **31**(18), 5811–5825 (2017) <https://doi.org/10.2298/FIL1718811Z>

Zou, X., Zheng, Y., Zhang, L., Lv, J.: Survivability and stochastic bifurcations for a stochastic Holling type II predator-prey model. *Communications in Nonlinear Science and Numerical Simulation* **83**, 105136 (2020) <https://doi.org/10.1016/j.cnsns.2019.105136>